Research Square

Preprints are preliminary reports that have not undergone peer review.
They should not be considered conclusive, used to inform clinical practice,
or referenced by the media as validated information.

The BMP-Krüppel-like factor 3 axis promotes resilience programming in exhausted CD8+ T cells

Hazem Ghoneim

Hazem.Ghoneim@osumc.edu

The Ohio State University College of Medicine https://orcid.org/0000-0002-9816-4286

Abbey Saadey

Ohio State University College of Medicine https://orcid.org/0009-0004-8473-1288

Amir Yousif

Ohio State University College of Medicine

Ava Lowin

The Ohio State University College of Medicine

Kelley Ptak

The Ohio State University College of Medicine

Madeline Allison

Ohio State University

Asmaa Yousif

The Ohio State University College of Medicine

Mykaila Johnson-Marable

Ohio State University College of Medicine

Chelsea Castillo

Ohio State University College of Medicine

Amy Webb

The Ohio State University Wexner Medical Center https://orcid.org/0000-0001-5503-7300

Article

Keywords: CD8 T cells, T cell exhaustion, BMP signaling, epigenetic programming, immune checkpoint blockade

Posted Date: November 24th, 2026

DOI: https://doi.org/10.21203/rs.3.rs-10357366/v1

License: This work is licensed under a Creative Commons Attribution 4.0 International License.
Read Full License

Additional Declarations: There is **NO** Competing Interest.

The BMP-Krüppel-like factor 3 axis promotes resilience programming in exhausted CD8+ T cells.

Abbey A. Saadey[1,2], Amir Yousif[1,3], Ava Lowin[1,2], Kelley Ptak[1], Madeline R. Allison[1,2], Asmaa M. Yousif[1], Mykaila Johnson-Marable[1,4], Chelsea Castillo[1], Amy Webb[5], Hazem E. Ghoneim[1,2,3,4,6]*

[1]Department of Microbial Infection and Immunity, College of Medicine, The Ohio State University; Columbus, OH, USA.

[2]Biomedical Sciences Graduate Program, College of Medicine, The Ohio State University; Columbus, OH, USA.

[3]Molecular, Cellular and Developmental Biology Graduate Program, College of Medicine, The Ohio State University; Columbus, OH, USA.

[4]Immunology and Microbial Pathogenesis Master's Program, College of Medicine, The Ohio State University; Columbus, OH, USA.

[5]Department of Biomedical Informatics, College of Medicine, The Ohio State University; Columbus, OH, USA.

[6]The Pelotonia Institute for Immuno-Oncology, James Comprehensive Cancer Center, The Ohio State University; Columbus, OH, USA.

*Corresponding author. Email: Hazem.Ghoneim@osumc.edu

ABSTRACT

T cell exhaustion limits durable cytotoxic CD8+ T cell responses during chronic infections and cancer and remains a major barrier to cancer immunotherapies, including immune checkpoint blockade (ICB). Defining the mechanisms that preserve CD8+ T cell fitness under chronic stimulation may reveal pathways that sustain immune competence and improve therapeutic invigoration. Here, we show that the transcription factor Krüppel-like factor 3 (KLF3) supports CD8+ T cell persistence, proliferative capacity, and progenitor-like programming during chronic viral infection and tumor challenge. KLF3 expression is progressively silenced as CD8+ T cells become terminally exhausted, whereas KLF3 restoration preserves progenitor exhausted T cells, enhances translational activity, and improves functional capacity. We further show that BMP-Smad1/5 signaling activation during TGFβR1 blockade restores KLF3 expression in dysfunctional T cells and enables their proliferative response to ICB in a KLF3-dependent manner. These findings reveal a BMP-KLF3 regulatory axis that sustains CD8+ T cell resilience during chronic infection and cancer and defines a targetable pathway for improving CD8+ T cell responses to immune checkpoint blockade.

KEYWORDS:

CD8 T cells, T cell exhaustion, BMP signaling, epigenetic programming, immune checkpoint blockade

INTRODUCTION

Cytotoxic CD8+ T cells are critical for controlling viral infections and cancer through antigen-specific killing of virus-infected or malignant cells. Upon antigen clearance, such as during acute viral infections, CD8+ T cells develop into long-lived memory T cells that provide immune surveillance and robust protection upon antigen re-encounter [1,2]. In contrast, during chronic infections or cancer, persistent antigen stimulation and inflammatory signals drive CD8+ T cells into exhaustion, preventing memory differentiation and limiting protective responses against chronic pathogens and tumors [1–3]. Exhausted T cells (TEX) are characterized by reduced cytotoxic effector function, impaired proliferation, metabolic dysfunction, and poor survival [4]. TEX cells also sustain high expression of inhibitory receptors (e.g., PD-1, CTLA-4), which restrain T cell activity and are major targets of immune checkpoint blockade (ICB) therapies [1,2,4]. Despite the success of ICB in treating several types of cancers, heterogeneity within TEX populations influences their functional capacity and immunotherapy responsiveness [5,6]. A key subset of TEX cells, known as progenitor exhausted T cells (Tprog), retains self-renewal capacity and provides the proliferative burst following ICB treatment [5–8]. Tprog cells serve as a renewable source for other TEX subsets, differentiating into either a cytolytic subset (Tcyto), which retains cytotoxic effector function and ICB responsiveness, or terminally exhausted (Tterm), which arise under persistent stimulation and are refractory to ICB [5,6,9,10].

Epigenetic programming of TEX cells plays a central role in stabilizing terminal exhaustion [11–13]. We and others have shown that key effector and memory-associated genes are progressively silenced in Tterm cells, locking their fate commitment while restricting their long-term fitness and ICB responsiveness [14–19]. Although persistent T cell receptor (TCR) signaling is essential for driving T cell exhaustion [20,21], our previous work identified opposing roles of transforming growth factor beta-1 (TGFβ1) and bone morphogenetic protein (BMP) signals in regulating the epigenetic programming of human and murine TEX cells [22]. Specifically, activating

BMP signaling while blocking TGFβ1 restored functionality in dysfunctional human CD8+ T cells, and enhanced murine TEX cell responses to ICB during chronic lymphocytic choriomeningitis virus (LCMV) infection [22]. However, the cell-intrinsic mechanisms by which these upstream signals promote or counteract exhaustion programming remains incompletely defined. Identifying the downstream mediators of BMP-dependent T cell fitness may reveal pathways that prevent terminal exhaustion and improve therapeutic responsiveness.

Our previous work revealed that rebalancing TGFβ1/BMP signals in dysfunctional human CD8+ T cells restored expression of the transcription factor Krüppel-like factor 3 (KLF3) [22]. KLF3 has known roles in B and T lymphocyte differentiation and homeostasis, often acting alongside the closely related factor KLF2 to regulate lymphocyte trafficking [23–25]. In TEX cells, recent studies have identified KLF2 as a key regulator of the progenitor-to-cytolytic transition during chronic infection and cancer [26–28]. Intriguingly, two studies showed that KLF3 deletion in antigen-specific CD8+ T cells favors KLF2-driven effector differentiation and migration during chronic viral infection [29] and disrupts tissue-resident memory programs during acute infection [30], suggesting that KLF3 can oppose KLF2-mediated CD8+ T cell programming. However, whether a BMP-KLF3 axis regulates TEX programming and responsiveness to immunotherapy remains unknown.

Here, we show that the KLF3 gene is epigenetically silenced in terminally exhausted CD8+ T cells undergoing chronic antigen and TGFβ1 stimulation. Restoring KLF3 expression in antigen-specific CD8+ T cells remodeled their transcriptomic programs and epigenomic DNA methylation landscape toward a functional, progenitor-like state that enhanced proliferative capacity and protein translation activity during chronic LCMV infection and cancer. Importantly, late activation of BMP signaling in dysfunctional CD8+ T cells recovered KLF3 expression and enhanced TEX proliferative responses to ICB therapy in a KLF3-dependent manner. Together, these findings reveal the BMP-KLF3 axis as a novel pathway that supports CD8+ T cell resilience during chronic infection and cancer.

RESULTS

KLF3 is epigenetically silenced in terminally exhausted CD8+ T cells

Terminal CD8+ T cell dysfunction is accompanied by stable transcriptional and epigenetic remodeling that limits functional recovery and responsiveness to ICB [10–19]. We previously found that terminally dysfunctional human CD8+ T cells, generated by chronic TCR stimulation in the presence of TGFβ1 signals ("Dysf.") [22], downregulated KLF3 relative to acutely stimulated CD8+ T cells (**Fig. 1A**). In contrast, combined inhibition of TGFβ receptor-1 signaling ("TGFβR1i") and activation of BMP-Smad1/5 signaling ("BMPa") restored KLF3 expression (**Fig. 1A**), coinciding with recovery of effector and memory-associated programs [22]. These observations suggested that KLF3 may be actively repressed during the acquisition of terminal dysfunction and re-expressed under conditions that restore exhausted CD8+ T cell fitness.

To determine whether KLF3 repression is a conserved feature of terminal exhaustion *in vivo*, we first examined KLF3 expression levels across virus-specific exhausted CD8+ T cell (TEX) states during chronic LCMV infection [9]. KLF3 expression was highest in the progenitor (Tprog) TEX subset and declined as TEX cells progressed toward terminal exhaustion (**Fig. 1B**). This transcriptional loss was accompanied by epigenetic remodeling at the *Klf3* locus. PD-1+ Tim3+ TEX cells from chronic LCMV showed reduced chromatin accessibility at the *Klf3* gene compared with naive, memory, and Tprog TEX CD8+ T cells [31] **(Fig. 1C**). Terminally dysfunctional ("$T_{Dysf.}$") mouse antigen-specific CD8+ T cells generated *in vitro* [32] showed a similar reduction in *Klf3* locus accessibility relative to functional acutely stimulated cells (**Fig. 1C**). Consistent with these murine datasets, exhausted tumor-infiltrating CD8+ T cells from multiple human cancers showed coordinated KLF3 downregulation and reduced chromatin accessibility compared with functional T cell populations [22,33,34]. Thus, KLF3 repression is a shared feature of terminal CD8+ T cell exhaustion across chronic viral infection, tumor microenvironment, and prolonged *in vitro* stimulation.

Because terminal exhaustion is reinforced by de novo DNA methylation [14], we next asked whether reduced accessibility at the *Klf3* locus was accompanied by acquisition of DNA methylation. During chronic LCMV infection, the *Klf3* locus gained DNA methylation in TEX cells (**Fig. 1C**), consistent with Dnmt3a-dependent de novo methylation programs that enforce exhausted CD8+ T cell differentiation [14]. These findings suggested that KLF3 is not merely downregulated as a consequence of T cell activation history but becomes epigenetically restrained as CD8+ T cells transition into a fixed, terminally exhausted state.

To define the kinetics of KLF3 repression, we employed our established *in vitro* model of terminal CD8+ T cell exhaustion using mouse P14 CD8+ T cells [32], which express a transgenic TCR specific for the LCMV GP33 epitope (**Fig. 1D**). In this model, repeated GP33 stimulation in the presence of TGFβ1 for about three weeks drives an epigenetically stabilized, terminal dysfunction state in P14 cells ("$T_{Dysf.}$"), whereas P14 cells acutely stimulated for 7 days ("Acute-7d") remain functionally competent [32]. $T_{Dysf.}$ P14 cells upregulated PD-1 and Tim3 inhibitory receptors compared to rested Acute-7d cells (**Extended Data Fig. 1A-B**), while progressively losing interferon-gamma (Ifnγ) cytokine production and CD107a degranulation capacity, with the deepest functional impairment observed by day 19 (**Fig. 1E-F**, **Extended Data Fig. 1C**).

KLF3 expression declined early during the transition toward dysfunction. By day 9, $T_{Dysf.}$ cells showed significant downregulation compared to rested Acute-7d cells, and KLF3 expression was further reduced by day 19 **(Fig. 1G**, **Extended Data Fig. 1D**). To determine whether this transcriptional repression coincided with DNA methylation remodeling, we performed targeted DNA methylation analysis using Oxford Nanopore technology of two key TEX-associated differentially methylated regions (DMRs) located within promoter and intronic regulatory regions of the *Klf3* locus (**Extended Data Fig. 1E**). Antigen-experienced P14 cells acquired de novo DNA methylation at both regions by day 9 compared to naïve cells, consistent with initial KLF3 repression after activation (**Extended Data Fig. 1D, 1F**). However, DNA methylation at both regions was further increased by day 19 in $T_{Dysf.}$ P14 cells compared to rested Acute-7d cells (**Fig.**

1H), indicating progressive epigenetic consolidation of KLF3 silencing during terminal dysfunction. Together, these data demonstrate that chronic antigen plus TGFβ1 stimulation progressively drives KLF3 repression as CD8+ T cells acquire terminal dysfunction. This repression is linked to loss of chromatin accessibility and increased DNA methylation at *Klf3* regulatory elements, placing KLF3 within the epigenetic circuitry that stabilizes terminal CD8+ T cell exhaustion.

Restoring KLF3 preserves progenitor-like CD8+ T cells during chronic viral infection

Because KLF3 was epigenetically silenced as CD8+ T cells progressed toward terminal exhaustion, we next asked whether enforced KLF3 expression could alter the fate of antigen-specific CD8+ T cells during chronic infection. Activated P14 cells were retrovirally transduced (RV) with either a KLF3 expression construct and an mCherry fluorescent reporter (KLF3 "overexpression", herein referred to as "KLF3-OE") or an empty vector GFP control ("Ctl") (**Extended Data Fig. 2A-B**). Transduced P14 cells were sorted based on reporter expression, and increased KLF3 expression was confirmed in KLF3-OE mCherry+ cells (**Extended Data Fig. 2C-D**). Congenically distinct KLF3-OE and Ctl P14 cells were then co-adoptively transferred at an equivalent ratio into Rag1-/- mice on day 2 post-chronic LCMV infection (p.i.) (**Fig. 2A, Extended Data Fig. 2E**), a model which drives severe and persistent exhaustion programming in virus-specific CD8+ T cells [14].

On day 9 p.i., KLF3-OE P14 cells showed a modest increase in abundance compared to Ctl cells, most prominently in the liver (**Extended Data Fig. 3A-D**). However, during a late stage of chronic infection (day 34 p.i.), enforced KLF3 expression established a striking competitive advantage, with KLF3-OE P14 cells becoming significantly more abundant than Ctl cells in the spleen, liver and lungs, and showing a greater fold increase relative to their corresponding day 9 numbers (**Fig. 2B-H**). This enhanced persistence was accompanied by altered TEX subset

distribution across lymphoid and non-lymphoid tissues. KLF3-OE cells were preferentially enriched within the Ly108+ Cx3cr1- progenitor TEX subset and showed reduced differentiation into the Cx3cr1+ cytolytic TEX subset (**Fig. 2I-J, Extended Data Fig. 3E-H**). Thus, KLF3 restoration did not simply induce an early expansion advantage but instead supported the persistence and maintenance of a progenitor-like reservoir under severe chronic stimulation, rather than accelerating terminal effector differentiation.

To more directly relate KLF3 protein abundance to TEX cell phenotype, we generated a second retroviral construct encoding 3xFLAG-tagged KLF3 (**Extended Data Fig. 4A**). Because mCherry is expressed from a separate promoter and may not faithfully report KLF3 protein abundance, FLAG staining allowed identification of cells with high KLF3 protein expression ("KLF3-FLAG-hi", gated as the top 20% of KLF3-FLAG+ cells) (**Extended Data Fig. 4B**). On day 30 p.i., KLF3-FLAG-hi P14 cells expressed significantly higher levels of the proliferation marker Ki67, Ly108, and the lymphoid tissue-homing marker Ccr7 than Ctl P14 cells (**Fig. 2K**, **Extended Data Fig. 4C-D**). KLF3-FLAG-hi cells also showed increased PD-1 expression, whereas Tim3 expression was not significantly different from Ctl cells (**Extended Data Fig. 4E-F**). Thus, KLF3 may not erase the exhausted state, but instead preserves proliferative and progenitor-associated features within chronically stimulated PD-1+ CD8+ T cells.

We then tested whether this progenitor-like phenotype was accompanied by improved function. Following *ex vivo* GP33 peptide stimulation of splenocytes, KLF3-FLAG-hi P14 cells showed significantly higher frequency of the Ifnγ+ Tnf+ polyfunctional population and expressed more Tnf cytokine than Ctl P14 cells (**Fig. 2L**, **Extended Data Fig. 4G**). KLF3-OE P14 cells also expressed more Perforin at day 34, whereas Ctl cells expressed higher levels of Granzyme B (Gzmb), consistent with a terminally TEX phenotype [35,36] (**Extended Data Fig. 4H-I**). Together, these findings demonstrate that restoring KLF3 expression preserves a proliferative, progenitor-like state in virus-specific CD8+ T cells that are functionally responsive during chronic infection.

KLF3-OE CD8+ T cells retain stemness and anti-tumor function in solid tumors

We next asked whether KLF3 could similarly shape tumor-specific CD8+ T cells responses against solid tumors *in vivo*. To compare KLF3-OE and Ctl cells within the same antigenic and tumor microenvironment (TME), congenically distinct KLF3-OE mCherry+ and Ctl-GFP+ P14 cells were co-adoptively transferred into C57BL/6 mice bearing GP33-expressing B16-F10 melanoma tumors, followed by phenotypic and functional analyses one week later (**Fig. 3A**). At this early timepoint, KLF3-OE P14 cells were more abundant in tumor-draining lymph nodes (tDLN), but less abundant within tumors compared to Ctl cells (**Extended Data Fig. 5A-B**), suggesting that KLF3-OE cells are preferentially maintained in lymphoid tissues early in the anti-tumor response. Despite reduced early tumor accumulation, KLF3-OE P14 cells showed a pronounced shift in differentiation state. Similar to chronic LCMV infection, KLF3-OE P14 cells were enriched within the Ly108+ Cx3cr1- progenitor-like compartment and showed reduced representation within Cx3cr1+ cytolytic and Ly108- Cx3cr1- terminal TEX subsets (**Fig. 3B-E**). Importantly, within tumors, KLF3-OE P14 TILs retained higher expression of Ki67 and the progenitor-associated transcription factor Tcf1 [7,31], while expressing lower levels of Tim3 and PD-1 (**Fig. 3F-H, Extended Data Fig. 5C**). These findings indicate that KLF3 restrains rapid terminal differentiation and helps sustain a progenitor-like state in tumor-specific CD8+ T cells.

We next assessed whether KLF3-OE tumor-infiltrating P14 cells maintained antigen-specific effector capacity. Following *ex vivo* GP33 peptide stimulation, KLF3-OE P14 TILs produced more Ifnγ than Ctl cells (**Fig. 3I-J**). To directly measure cytotoxic activity, we utilized our established *in vitro* tumor killing assay [22,32] in which chronically GP33 plus TGFβ1-stimulated Ctl or KLF3-OE P14 cells were co-cultured with GP33-expressing CT2A glioma cells (**Fig. 3K**). Both P14 conditions killed tumor targets after 18-hours, yet KLF3-OE P14 cells induced approximately two-fold greater tumor cell death than Ctl P14 cells (**Fig. 3L**). Thus, KLF3 restoration preserves stem-like features without compromising cytotoxic potential.

We next tested whether KLF3 expression improved tumor control *in vivo*. We adoptively transferred either Ctl-GFP+ or KLF3-OE mCherry+ P14 cells into C57BL/6 mice bearing B16-F10-GP33 tumors and monitored tumor growth over time (**Extended Data Fig. 5D**). Mice receiving KLF3-OE P14 cells showed significantly reduced average tumor volume compared to recipients of Ctl P14 cells (**Extended Data Fig. 5E-F**). At endpoint, KLF3-OE P14 cells were more abundant in tDLNs and trended higher within tumors (**Extended Data Fig. 5G-H**). Consistent with the early co-transfer analysis, KLF3-OE P14 cells retained higher frequency of the progenitor-like cells and a reduced frequency of the cytolytic TEX cells within the TME (**Extended Data Fig. 5I-K**). To benchmark KLF3-OE and Ctl P14 cells against endogenous tumor-infiltrating CD8+ TEX populations, we compared their Ly108 and Cx3cr1 expression with polyclonal endogenous TEX subsets within the same B16 tumors. KLF3-OE P14 cells displayed Ly108 expression similar to endogenous Tprog cells, whereas Ctl P14 cells more closely resembled the Cx3cr1 expression pattern of the Tcyto subset (**Extended Data Fig. 5L-M**). In addition, KLF3-OE P14 TILs maintained lower PD-1 and Tim3 expression and higher Ifnγ production than Ctl P14 cells at tumor endpoint (**Extended Data Fig. 5N-P**). Together, these data indicate that restoring KLF3 expression remarkably improves anti-tumor CD8+ T cell fitness by preserving a progenitor-like, functionally responsive state while restraining terminal differentiation within the TME.

Restoring KLF3 promotes progenitor-like transcriptional programming in CD8+ T cells

We next sought to define transcriptional changes induced by KLF3 restoration in chronically stimulated CD8+ T cells. KLF3-OE and Ctl P14 cells were isolated from chronic LCMV-infected Rag1-/- mice on day 9 or day 34 p.i. and analyzed by ultra-low input RNA sequencing (**Fig. 4A**). Principal component analysis (PCA) and differential gene expression analysis showed little separation between KLF3-OE and Ctl P14 cells on day 9 p.i., consistent with the modest phenotypic differences observed at this early time point (**Fig. 4B**, **Extended Data Fig. 6A**). However, during the chronic stage on day 34 p.i., KLF3-OE and Ctl cells were transcriptionally

distinct, with 698 differentially expressed genes (DEGs) upregulated and 785 genes downregulated in KLF3-OE P14 cells compared to Ctl cells (**Fig. 4B-C, Extended Data Fig. 6A**). Thus, restoring KLF3 expression establishes a distinct transcriptional state in CD8+ T cells exposed to prolonged chronic stimulation.

Genes upregulated in KLF3-OE cells were associated with progenitor-like differentiation, TCR signaling, costimulation, cytokine production, chromatin regulation, and protein translation (**Supplementary Table 1**). The upregulated DEGs included the stemness-associated transcription factor *Lef1* [37], TCR/NF-kB and NFAT pathway-related genes, such as *Rel*, *Nfkbil1*, and *Nfat5*, the cell cycle regulator *E2f1*, the DNA demethylase *Tet3* and the histone demethylase *Kdm6b*. KLF3-OE cells also upregulated *Ifng* and *Il21*, a cytokine that supports T cell effector function and memory programs [38,39] together with *Foxo3*, which has been shown to promote IL-21 expression in follicular helper T (T_{FH}) cells [40] (**Fig. 4C**). Additional upregulated DEGs included *Furin* and *Cd27*, which have been linked to T cell effector and memory responses [41,42], and costimulatory molecules *Tnfsf4* (OX40-ligand) and *Tnfrsf9* (4-1BB) that support T cell expansion and function [43]. Notably, KLF3-OE cells also showed high expression of multiple ribosomal protein genes (e.g., *Rpl10a*, *Rps15*, *Rpl8*, etc.) (**Fig. 4C**). Importantly, many of these upregulated DEGs overlapped with the published transcriptional signature for the progenitor TEX subset during chronic LCMV infection [44], including the chemokine *Cxcl10*, NF-κB signaling regulators, *Ikzf2, Tnfsf4, Cd27, Nfat5*, and ribosomal protein genes (**Fig. 4D**). Moreover, KLF3-OE cells had increased expression of *Pou2f2* and *Tle3*, factors linked to progenitor TEX and memory CD8+ T cell states [45,46] (**Fig. 4D**). Gene set enrichment analysis (GSEA) confirmed positive enrichment of the KLF3-OE profile for the progenitor TEX signature [44] (**Extended Data Fig. 6B**). These findings indicate that KLF3 restoration promotes a progenitor-like transcriptional program during chronic viral infection.

In contrast, genes downregulated in KLF3-OE cells on day 34 p.i. were associated with cytolytic differentiation, terminal exhaustion, interferon signaling, and apoptosis (**Supplementary**

Table 1). These included *Gzmb*, *Ikzf3*, *Prdm1* encoding Blimp-1, *Klf2* and its target gene *S1pr1*, *Tbx21*, *Klrk1* encoding the NKG2D receptor, *Il18r1*, and the pro-apoptotic galectin genes *Lgals1* and *Lgals3* [47–50] (**Fig. 4C**). KLF3-OE cells also showed reduced expression of several interferon signaling-related genes, including *Ifit2*, *Ifit3*, *Jak1/2*, *Stat5a*, *Tbk1*, *Oasl2*, and *Irf7*, a transcription factor associated with terminal exhaustion [51] (**Fig. 4C**). Several downregulated genes overlapped with a cytolytic TEX transcriptional signature, and GSEA showed negative enrichment of the KLF3-OE profile for this signature [44] (**Fig. 4E, Extended Data Fig. 6C**). Notably, more than half of the upregulated and downregulated DEGs in KLF3-OE cells overlapped with genes bound by KLF2 in antigen-specific CD8+ T cells during chronic LCMV [29] (**Fig. 4F-G**), suggesting a subset of KLF3-regulated transcriptional changes may involve altered KLF2-dependent regulation, whereas others may occur through KLF2-independent mechanisms.

Pathway enrichment analysis further supported this transcriptional remodeling. Upregulated DEGs in KLF3-OE cells were enriched for protein translation pathways, consistent with their increased expression of ribosomal protein and ribosomal biogenesis genes (**Fig. 4C-D, Fig. 4H**). Conversely, downregulated DEGs were enriched for mitotic spindle, G2-M checkpoint, interferon gamma response, and interferon alpha response pathways (**Fig. 4I**). Together, these findings indicate that early KLF3 restoration promotes a progenitor-like transcriptional state, marked by enhanced protein translation-associated programming and reduced cytolytic/terminal exhaustion-associated gene expression during chronic stimulation.

KLF3-OE remodels exhaustion-associated DNA methylation programming in CD8+ T cells

De novo DNA methylation is a fundamental epigenetic mechanism that reinforces TEX programming [14]. Therefore, we next asked whether KLF3 restoration alters DNA methylation profiles in chronically stimulated CD8+ T cells. We performed whole genome bisulfite sequencing (WGBS) on KLF3-OE or Ctl P14 cells isolated on day 34 of chronic LCMV infection (**Fig. 5A**). Principal component analysis showed that KLF3-OE and Ctl P14 cells acquired distinct DNA

methylation profiles. KLF3-OE cells clustered closer to the endogenous Tprog subset along PC2, whereas Ctl cells more closely resembled Tcyto and Tterm subsets (**Fig. 5B**). KLF3-OE P14 cells showed extensive DNA methylation remodeling compared to Ctl cells, with ~1800 hypomethylated and ~2900 hypermethylated regions (**Fig. 5C**, **Supplementary Table 2**). Thus, KLF3 restoration is associated with broad remodeling of exhaustion-linked DNA methylation landscapes.

To identify regulatory features associated with these DMRs, we performed HOMER enrichment analysis. Hypomethylated regions in KLF3-OE cells were enriched for TF motifs associated with proliferation, differentiation, TCR signaling, and progenitor-associated regulation, including E2F, ETS, IRF3, Sp/KLF family members (Sp1, Klf17) , Runx1, GATA, NFAT:AP1 complex, and NFκB2 motifs [26,31,52–54] (**Fig. 5D**). In contrast, hypermethylated regions showed a more restricted motif profile, including TCF7L2, NFE2L2 that encodes NRF2, a TF previously linked to driving T cell exhaustion [55], Oct11 and Six2 motifs (**Fig. 5D**). These data suggest that KLF3 restoration remodels DNA methylation programs at regulatory elements enriched for TF motifs linked to T cell signaling, proliferation, and progenitor maintenance.

At the gene level, hypermethylated regions in KLF3-OE P14 cells were associated with loci including *Tgfbr2* and *Klf8* (**Fig. 5E**, **Extended Data Fig. 6D**), the latter of which has been shown to be actively repressed by KLF3 [56]. Conversely, hypomethylated regions were found near genes associated with T cell function, stemness, BMP signaling, and protein translation, including *Il21*, the BMP type II receptor *Acvr2a*, the progenitor-associated transcription factor *Bach2* [57], and the ribosomal protein gene *Rpl10* (**Fig. 5F-G and Extended Data Fig. 6E-F**). Integration with RNA-seq data showed that key genes containing hypomethylated DMRs in KLF3-OE cells tended to have higher RNA expression, whereas genes containing hypermethylated DMRs tended to have lower expression (**Extended Data Fig. 6G-H**), linking KLF3-associated methylation remodeling with transcriptional output. A subset of the DMR-associated genes also overlapped with genes bound by KLF2 in CD8+ T cells during chronic LCMV infection [29]. Hypomethylated

KLF2-bound genes included *Bach2*, *Bcl2*, *Jun*, *Pou2f2* and *Ets1* (**Extended Data Fig. 6I**), whereas hypermethylated KLF2-bound genes included *Prdm1*, *Tgfbr2*, *Irf8*, the stemness repressor *Bcor* [45], and several other KLF family TFs (**Extended Data Fig. 6J**), suggesting that DNA methylation changes within these genes could be linked to KLF3/KLF2 binding competition [29]. Together, these results reveal that KLF3 restoration reprograms exhaustion-associated DNA methylation at genes involved in CD8+ T cell function, progenitor programming, BMP signaling, and protein translation, with a subset of these changes occurring at loci bound by KLF2.

KLF3 enhances protein translation activity in chronically stimulated CD8+ T cells

Protein translation is required to sustain effector activity and proliferation in CD8+ T cells responding to infections or tumors, yet becomes impaired in TEX cells [35,58–62]. As such, we previously found that $T_{Dysf.}$ P14 CD8+ T cells lose their translational capacity compared to functional, acutely-stimulated cells [32]. As KLF3-OE cells showed enrichment of translation and ribosomal biogenesis pathways, we directly tested whether KLF3 restoration enhances protein translation activity using puromycin-incorporation assay. Splenocytes from chronic LCMV-infected Rag1-/- mice, which had received co-adoptively transferred Ctl and KLF3-FLAG transduced P14 cells on day 2 p.i., were stimulated *ex vivo* with GP33 peptide and analyzed by puromycin incorporation on day 30 p.i. (**Fig. 6A**). Being a structural analog to aminoacyl-tRNA, puromycin incorporation into nascent polypeptides provided quantitative flow cytometric measurement of active protein synthesis during antigen stimulation [63] (**Fig. 6A**). Indeed, KLF3-FLAG-hi P14 cells showed significantly higher puromycin incorporation than Ctl cells overall and were enriched within the Puro-hi subset, with corresponding reductions in the intermediate (Puro-int) and Puro-low subsets (**Fig. 6B-F**). In both Ctl and KLF3-FLAG-hi P14 cells, puromycin incorporation positively correlated with Ifnγ and Tnf expression, linking increased translational activity with production of effector cytokines (**Fig. 6G-J**). Thus, restoring KLF3 enhances protein

translation activity in chronically stimulated CD8+ T cells, providing a functional mechanism by which KLF3 supports improved effector protein production during chronic infection.

BMP activation recovers KLF3-dependent proliferative capacity in dysfunctional CD8+ T cells

As combined BMP-Smad1/5 activation and TGFβR1 blockade restored KLF3 expression in chronically stimulated human CD8+ T cells [22] (**Fig. 1A**), we sought to determine whether this treatment strategy could also recover KLF3 expression in $T_{Dysf.}$ P14 cells. P14 cells were treated with either TGFβR1 inhibitor "R", BMP-Smad1/5 agonist "A", or combined "R+A" starting from day 14 to day 18 of chronic GP33 plus TGFβ1 stimulation (**Fig. 7A**). As TGFβ1 signaling competes for co-Smad binding and can override BMP-Smad1/5 activity [22,64], combined TGFβR1 inhibitor and BMPa treatment was required to fully activate BMP signaling. The R+A-treated P14 cells remarkably recovered KLF3 expression to levels comparable to rested Acute-7d P14 cells, whereas monotherapy failed to restore KLF3 above $T_{Dysf.}$ levels (**Fig. 7B**). Although TGFβR1 inhibition alone partially restored $T_{Dysf.}$ P14 cell function, recovery was most pronounced with R+A treatment, which increased the frequency of Ifnγ+ CD107a+ cells to levels similar to rested Acute-7d P14 cells, and enhanced Perforin expression (**Extended Data Fig. 7A-C**). R+A treatment also significantly increased Ki67 expression (**Fig. 7C**), indicating that combined BMP activation and TGFβR1 inhibition restores KLF3 expression together with functional and proliferative activity in $T_{Dysf.}$ CD8+ T cells.

To determine whether late KLF3 recovery is required for R+A-mediated rescue of $T_{Dysf.}$ P14 cells, we deleted KLF3 in P14 cells by CRISPR-Cas9 after initial TCR activation using sgRNAs targeting two common exons [29] "KLF3-KO", with a non-targeting sgRNA as the scrambled control "Scr-Ctl" (**Fig. 7D**). KLF3-KO cells showed efficient editing at both target regions within the *Klf3* locus (**Extended Data Fig. 7D-E**). CRISPR-edited P14 cells were then stimulated with GP33 peptide and TGFβ1 followed by R+A treatment until day 21 (**Fig. 7D**). In

Scr-Ctl P14 cells, R+A treatment increased Ki67 expression relative to mock-treated $T_{Dysf.}$ cells, while this proliferative response was lost in R+A-treated KLF3-KO P14 cells (**Fig. 7E**). In contrast, both Scr-Ctl and KLF3-KO P14 cells showed functional recovery after R+A treatment, including increased frequency of Ifnγ+ CD107a+ cells and Perforin expression compared to mock-treated $T_{Dysf.}$ cells (**Extended Data Fig. 7F-G**). These findings indicate that KLF3 is required for the proliferative response induced by BMP activation/TGFβR1 blockade, whereas effector-function recovery can occur through KLF3-independent pathways downstream of this treatment strategy.

KLF3 deficiency limits BMP-driven CD8+ T cell proliferative response to ICB therapy

Finally, we asked whether KLF3 is required for the beneficial effects of R+A treatment on CD8+ T cell programming and responsiveness to ICB therapy during chronic LCMV infection [22]. Congenically distinct, CRISPR-edited Scr-Ctl and KLF3-KO P14 cells were co-adoptively transferred into chronic LCMV-infected Rag1-/- mice, followed by mock or TGFβR1i plus BMPa (R+A) treatment during the chronic stage of infection (day 20-27), and subsequently by PD-L1 blockade (ICB) therapy beginning on day 29 p.i. (**Fig. 7F**). Although combined R+A and aPD-L1 treatment increased overall P14 cell numbers across analyzed tissues compared with mock + aPD-L1 (**Extended Data Fig. 8A**), this effect was driven primarily in Scr-Ctl P14 cells. KLF3-KO cells showed only a modest non-significant increase in cell number following ICB therapy (**Fig. 7G, Extended Data Fig. 8A**). Importantly, R+A treatment also significantly increased the numbers of Ki67+ proliferating Scr-Ctl P14 cells in the spleen but had little effect on KLF3-KO cells (**Fig. 7H**). Consistently, KLF3-KO cells maintained lower Ki67 expression than Scr-Ctl regardless of treatment condition (**Fig. 7I**). Although Scr-Ctl and KLF3-KO P14 cells showed minimal differences in the Ly108/Cx3cr1 TEX subset distribution following ICB therapy (**Extended Data Fig. 8B-C**), Ki67 expression was consistently reduced in KLF3-KO cells across all three TEX

subsets (**Extended Data Fig. 8D**). These data indicate that KLF3 is required for the proliferative expansion induced by R+A treatment during ICB therapy.

KLF3 deficiency also impaired features linked to progenitor maintenance, effector function, and translational activity. KLF3-KO P14 cells showed reduced Ccr7 expression compared to Scr-Ctl P14 cells (**Fig. 7J**), opposite to the effect observed with KLF3 overexpression. KLF3-KO P14 cells also showed modestly reduced PD-1 and Tim3 expression, including a lower frequency of Tim3+ cells (**Extended Data Fig. 8E-F**). Following *ex vivo* GP33 peptide stimulation, Scr-Ctl P14 cells showed significantly higher numbers of polyfunctional Ifnγ+ Tnf+ cells than KLF3-KO cells, but only in R+A-treated mice (**Fig. 7K**). Finally, KLF3-KO P14 cells showed reduced frequency of the Puro-hi subset and increased frequency of the Puro-low subset compared to Scr-Ctl cells following puromycin incorporation during stimulation (**Fig. 7L**, **Extended Data Fig. 8G**). The Puro-low subset produced the lowest levels of effector molecules, including Tnf, Perforin and Gzmb, compared to Puro-hi and –int subsets (**Extended Data Fig. 8H-J**). Collectively, these findings indicate that KLF3 is required for chronically stimulated CD8+ T cells to mount the enhanced proliferative, functional, and protein translational responses induced by combined BMP activation and TGFβR1 blockade during ICB therapy.

DISCUSSION

Durable CD8+ T cell immunity during chronic infection and cancer depends on the maintenance of progenitor TEX cells that can self-renew, persist, and generate effector progeny under persistent antigen stimulation [5,7–10]. In contrast, terminally exhausted TEX cells acquire stable transcriptional and epigenetic programs that restrict proliferative capacity and limit responsiveness to ICB therapy [5,6,9–19]. In this study, we have shown that KLF3 is progressively silenced as CD8+ T cells transition toward terminal exhaustion, and that restoring KLF3 preserves a progenitor-like, translationally active, and ICB-responsive CD8+ T cell state under persistent antigen stimulation. KLF3 repression was observed in TEX cells in three systems: chronic LCMV

infection, tumors, and *in vitro*-generated terminal dysfunction. In all cases, downregulation of KLF3 protein and transcripts was associated with reduced chromatin accessibility and increased DNA methylation at the *Klf3* locus [14,22,31–34]. Our kinetic analysis further showed that KLF3 repression begins early during chronic stimulation and becomes more pronounced as CD8+ T cells develop terminal dysfunction, suggesting that KLF3 silencing is embedded within the epigenetic remodeling that stabilizes terminal dysfunction.

Restoring KLF3 altered the fate of antigen-specific CD8+ T cells during chronic infection and tumor challenge. In the chronic LCMV infection setting, KLF3-OE P14 cells showed enhanced persistence at late stages of infection and were preferentially maintained within the progenitor TEX compartment, with reduced terminal differentiation. While KLF3-expressing CD8+ T cells retained features of chronic stimulation, including PD-1 expression, they showed increased Ly108, Ccr7, Ki67, and polyfunctional cytokine production, indicating preservation of a less terminally differentiated yet functional state [8,10,65]. In GP33-expressing B16 melanoma, KLF3-OE P14 cells similarly retained higher Tcf1 and Ki67 expression, produced more effector molecules, showed stronger tumor killing activity during chronic stimulation, and improved tumor control *in vivo*. These findings suggest that KLF3 supports CD8+ T cell fitness by preserving developmental plasticity without eliminating effector potential, a balance likely needed for durable responses in chronic infections and cancer [6,66,67].

Transcriptional, epigenetic, and translational analyses further support this model. KLF3 restoration re-wired transcriptional programs in CD8+ T cells, which were enriched for progenitor TEX-associated genes, TCR and costimulatory signaling, cytokine-associated programs, chromatin regulators, and ribosomal protein genes, while showing reduced expression of genes linked to terminal exhaustion, interferon signaling, apoptosis, and circulation-associated programs. KLF3-OE cells also acquired DNA methylation profiles more similar to endogenous Tprog cells, with hypomethylated regions enriched for motifs linked to proliferation, TCR signaling, and progenitor-associated regulation, including E2F, ETS, NFAT:AP1, and NFκB-related motifs.

Integration with RNA expression suggested that these epigenetic changes are linked to transcriptional output at genes involved in T cell function, BMP signaling, stemness, and protein translation. Functionally, KLF3-FLAG-hi cells showed increased puromycin incorporation during antigen restimulation, and translation activity correlated with effector cytokine expression. Thus, KLF3 may support exhausted CD8+ T cell fitness not only by shaping transcriptional and epigenetic landscapes, but also by preserving the biosynthetic capacity needed to convert transcriptional potential into effector protein production [58,60].

These findings also build on our previous work defining BMP and TGFβ signaling as upstream regulators of CD8+ T cell exhaustion programming [22,32]. Combined BMP-Smad1/5 activation and TGFβR1 blockade restores effector function, cytotoxicity, and self-renewal capacity in chronically stimulated human CD8+ T cells, along with expanding TEX cells in response to ICB during chronic infection [22]. KLF3 recovery is an important CD8+ T cell-intrinsic mechanism downstream of this pathway, particularly for restoring proliferative and biosynthetic fitness. BMP-agonist plus TGFβR1 inhibitor treatment restored KLF3 expression in terminally dysfunctional P14 cells, along with improved effector function and Ki67 induction. However, KLF3 deletion selectively impaired the proliferative response while leaving much of the effector-function rescue intact *in vitro*, indicating that KLF3 is not a universal mediator of BMP activation/TGFβ1 blockade-driven recovery. *In vivo*, KLF3 deficiency limited antigen-specific CD8+ T cell expansion after combined BMPa plus TGFβR1i treatment and PD-L1 blockade, reduced Ki67 expression across TEX subsets, impaired polyfunctional cytokine responses, and decreased translational activity. These new findings are consistent with broader roles for BMP signaling in regulating KLF-family transcription factors in progenitor-cell contexts [68,69]. In addition, prior work showed reciprocal regulation between KLF3 and KLF2, with KLF2 promoting effector-like differentiation in acute infection, CAR T cells, and chronic infection, while KLF3 opposed KLF2-associated cytolytic TEX programming through competition at shared chromatin binding sites [27–30]. Our data are consistent with a model in which KLF3 restrains cytolytic differentiation without abolishing effector potential.

Thus, BMP-dependent recovery of KLF3 may help maintain the balance between progenitor maintenance and functional capacity that is required for durable responses to ICB. This axis may be particularly relevant to adoptive T cell therapies, where preserving stem-like fitness while maintaining effector competence remains a central challenge [70,71].

Several limitations should be considered when interpreting these findings. Although the KLF3-FLAG system linked KLF3 protein abundance to phenotype, bulk transcriptomic and epigenomic analyses were performed on reporter-positive KLF3-OE P14 cells that could not be stratified by KLF3 protein level, as intracellular FLAG staining was incompatible with live cell sorting. Thus, some transcriptional and DNA methylation changes may reflect direct KLF3-dependent regulation, whereas others may result indirectly from altered cell state, enhanced translation-associated programming, or increased effector protein production. In addition, systemic BMP activation and TGFβR1 blockade may affect multiple immune, stromal, and tissue compartments and may not activate BMP signaling uniformly across antigen-specific P14 cells. Finally, although CRISPR-mediated deletion supports a role for KLF3 in TEX cell proliferative recovery, KLF3-KO cells could not be purified exclusively for successfully edited cells, which may underestimate the impact of KLF3 deficiency. Future studies using endogenous polyclonal CD8+ T cells, engineered T cell therapies, conditional genetic models, and direct chromatin occupancy approaches will be important for defining the physiological breadth and direct regulatory mechanisms of KLF3-dependent programming.

ACKNOWLEDGMENTS

We would like to thank the members of the Ghoneim Lab and colleagues at The Ohio State University for their support and feedback throughout this study. We thank VectorBuilder for providing the retroviral constructs used in this study, and the National Institutes of Health (NIH) Tetramer Core Facility at Emory University in Atlanta, GA for providing the GP33 tetramers used for the detection of LCMV-specific P14 CD8+ T cells. Funding support for this study was

provided by the National Institute of Allergy and Infectious Diseases grant R01AI170926 (HEG), the National Institutes of Health training program 5T32AI165391 “Interdisciplinary Program in Microbe-Host Biology” (AAS), and The Ohio State University College of Medicine and Comprehensive Cancer Center funding (HEG).

AUTHOR CONTRIBUTIONS

Conceptualization: HEG, AAS; Methodology: HEG, AAS; Investigation: HEG, AAS, AY, AL, KP, MRA, AMY, MJM, CC, AW; Visualization: HEG, AAS; Funding acquisition: HEG, AAS; Supervision: HEG; Writing: HEG, AAS

COMPETING INTERESTS

The authors declare no competing interests.

METHODS

Ethics and study design

All experiments in this study were performed using transgenic mouse CD8+ T cells (P14) for *in vitro* chronic stimulation, *in vivo* chronic viral infection, or *in vivo* solid tumor mouse models according to The Ohio State University Institutional Animal Care and Use Committee (IACUC) protocol #2019A00000055-R2. All experiments were repeated at least 2-3 times using biologically independent samples, using both male or female mice to account for sex as a biological variable. Technical replicates for each experiment and their associated statistical analyses are indicated in the figure legends.

Animal housing procedures

All mice used for the P14 *in vitro*, chronic LCMV infection, and tumor models were housed at The Ohio State University following IACUC guidelines under the approved protocol #2019A00000055-

R2. The housing facility was kept within a standard temperature range (68°C–76°C), relative humidity 30-70%, and a 12-hour dark/light cycle (light 6 am to 6 pm). All mice throughout this study were fed standard Teklad 7912 chow (Envigo). C57BL/6 mice were ordered from Jackson Laboratory at 6-8-weeks old. Rag1-/- mice were initially received from Jackson Laboratory and bred in-house after confirming lack of endogenous lymphocytes by flow cytometry. P14 transgenic mice on C57BL/6 background were bred in-house after confirming Thy1.1/Thy1.2 expression and GP33 specificity by tetramer staining. Mice used for all experiments were at least 6-8 weeks old, and all experiments were repeated equally using male or female mice to account for sex as a biological variable. Recipient mice for adoptive transfer experiments were sex-matched with the donor mice. The reported findings throughout this study were consistent when using either male or female mice. At experiment endpoints (or as animals reached early removal criteria), mice were humanely euthanized following IACUC procedures.

Mouse *in vitro* CD8+ T cell terminal dysfunction model

In vitro chronic stimulation of mouse antigen-specific P14 CD8+ T cells was performed as previously described [32]. Naive CD8+ T cells were isolated from spleens of P14 transgenic mice using the EasySep Mouse CD8+ T Cell Isolation Kit (StemCell Technologies) and confirmed for GP33 antigen specificity by tetramer staining (NIH Tetramer Core Facility). Naive cells were activated from day 0-2 in 6-well plates (1-3x10^6 cells per well) coated with purified anti-mouse CD3 (5 µg/ml) and anti-mouse CD28 (10 µg/ml; BioLegend) in complete RPMI medium (10% fetal bovine serum, 1X penicillin-streptomycin; Gibco) plus recombinant human IL-2 (200 IU/ml; PeproTech) and 2-Mercaptoethanol (50 µM; MilliporeSigma). Following activation, P14 cells were seeded into 96-well U-bottom plates at a density of 2x10^5 cells per 200 µl and stimulated with GP33 peptide (0.3 µg/ml) in complete RPMI medium plus IL-2 (20 IU/ml), recombinant human IL-15 (10 ng/ml; PeproTech), and 2-Mercaptoethanol (50 µM). Fresh GP33 peptide-containing complete medium was replenished every 2-3 days throughout the experiment. Starting on day 7, GP33 peptide was removed from the medium for the Acute-7d condition through the remainder

of the experiment. For the $T_{Dysf.}$ condition, recombinant human TGFβ1 (5 ng/ml; PeproTech) was added to the GP33 peptide-containing complete medium starting on day 7 through the remainder of the experiment. For treatment experiments in **Fig. 7**, $T_{Dysf.}$ P14 cells were treated with RepSox (TGFβ receptor-1 inhibitor "TGFβR1i", 25 uM; MedChemExpress) and/or SB4 (BMP4 agonist "BMPa", 10 μM; MedChemExpress) in addition to TGFβ1 and GP33 peptide-containing complete medium starting from day 14 or 16 through the remainder of the experiment.

Quantitative real-time PCR (qRT-PCR)

To measure KLF3 RNA expression within *in vitro*-stimulated P14 cells, total RNA was first isolated from collected cell pellets using the AllPrep DNA/RNA Micro Kit (Qiagen). Messenger RNA was converted into complementary DNA (cDNA) using the High-Capacity RNA-to-cDNA Kit (Applied Biosystems), then used immediately for qRT-PCR. Primers for KLF3 (exon 1-3) and the housekeeping gene Beta-2 microglobulin were obtained as predesigned PrimeTime qPCR Primer Assays from Integrated DNA Technologies (IDT). The cDNA samples were split into triplicate wells per sample for each gene in 96-well plates, then mixed with the indicated primers at 1X concentration and SYBR Green Master Mix (BioRad). The qRT-PCR amplification was performed using the C1000 Touch thermocycler (BioRad) with standard cycling mode. The resultant cycle threshold (Ct) quantification values were used to calculate relative fold changes in KLF3 expression ($2^{-\Delta\Delta Ct}$).

Targeted DNA methylation sequencing

For targeted DNA methylation sequencing at *Klf3* loci, genomic DNA was first isolated from cell pellets using the AllPrep DNA/RNA Micro Kit (Qiagen). Bisulfite conversion was performed on the genomic DNA using the EZ DNA Methylation-Direct Kit (Zymo) to convert all unmethylated cytosine nucleotides to thymine. PCR amplification was performed on the bisulfite-converted DNA with JumpStart Taq DNA Polymerase (MilliporeSigma) and primers specific for the indicated regions (*Klf3* intron FP: 5'-GTGGTGTTGGGGGGGAAGTATG-3', RP: 5'-CAAAATCCATTTAAAATCCCACCCAC-3'; *Klf3* promoter FP: 5'-

GAAGTGAGAATGGTGAATTTATAGG-3', RP: 5'-CACACTTTAAAAACCTCAAAACAC-3') using an ABS Proflex Thermocycler (Applied Biosystems). PCR products were run on 2% agarose gels with ethidium bromide to confirm amplification of the predicted band sizes, then isolated using the Zymoclean Gel DNA Recovery Kit (Zymo). The purified PCR bands were then used for library prep with the Native Barcoding Kit 24 V14 and loaded onto R10 flow cells on a MinION Mk1D sequencer (Oxford Nanopore). The resultant FASTQ files were generated using Oxford Nanopore MinKNOW software (Version 25.09.16). FASTQ files underwent barcode trimming, genome alignment, and calculation of percent CpG methylation using an established NanoEM pipeline [22,32,72].

Retroviral vector generation

All retroviral constructs were designed using VectorBuilder services. For KLF3-OE and KLF3-FLAG expression plasmids, the mouse *Klf3* full coding sequence was added under the murine stem cell virus (MSCV) Ψ+ promoter and Kozak sequence to initiate transcription, followed by the human phosphoglycerate kinase (hPGK) promoter before the mCherry fluorescent protein sequence. The KLF3-FLAG construct incorporated the 3xFLAG epitope sequence on the N-terminus end of the *Klf3* coding sequence. For the empty vector control (Ctl) plasmid, the green fluorescent protein (GFP) sequence was added under the MSCV Ψ+ promoter and Kozak sequence. All plasmid designs included the ampicillin resistance gene for bacterial growth selection. Plasmids were expanded from transformed *Escherichia coli* bacterial glycerol stocks streaked on LB agar plates containing ampicillin (50 µg/ml; MilliporeSigma) overnight at 37 °C, followed by isolation of individual colonies and overnight expansion in LB broth containing ampicillin (80 µg/ml) at 37 °C with shaking at 220 rpm. Plasmid DNA was extracted from the liquid bacterial cultures using the Nucleospin Plasmid kit (Macherey-Nagel).

To generate retrovirus (RV)-containing supernatants by transfection, plat-E cells (kindly received from Dr. Ken Oestreich at The Ohio State University, originally from Cell Biolabs, Inc.) were grown in complete DMEM medium (with 10% FBS and 1X P/S). One day prior to

transfection, $1x10^6$ plat-E cells were seeded into 6-well plates in complete, antibiotic-free DMEM. At 60-70% confluency, plat-E cells were transfected with either KLF3-OE or Ctl plasmid at a 2:1 ratio with the packaging plasmid pCL-Eco (AddGene) (12 µg total plasmid DNA per well) in Opti-MEM medium (Gibco) containing polyethyleneimine (PEI, 36 µg per well; MilliporeSigma). At 4-6 hours following transfection, the plat-E medium was replaced with fresh complete, antibiotic-free DMEM. RV-containing supernatants were collected at 24 and 48 hours post-media change. The collected supernatants were adjusted to 4x concentration by overnight precipitation using polyethylene glycol (PEG)-8000 (MilliporeSigma) following the described process [73]. Concentrated RV supernatants were resuspended in sterile DMEM and frozen at –80 °C.

Retroviral transduction of mouse P14 CD8+ T cells

For chronic infection and tumor experiments using KLF3-OE or Ctl P14 cells, retroviral transduction was performed according to the described process [74]. Naive CD8+ T cells were isolated from spleens of P14 transgenic mice using the EasySep Mouse CD8+ T Cell Isolation Kit (StemCell Technologies). The naive P14 cells were seeded into anti-CD3 (5 µg/ml) and anti-CD28 (10 µg/ml) coated 6-well plates at a density of $1\text{-}3x10^6$ cells per well in complete RPMI medium containing recombinant human IL-2 (200 IU/ml) and 2-Mercaptoethanol (50 µM). After 18-20 hours, the P14 cells were collected from the 6-well plates, and Percoll (Cytiva) gradient centrifugation was performed to select for activated cells [74]. Activated P14 cells were seeded into 96-well, non-TC treated flat-bottom plates coated one day prior with recombinant human fibronectin (“RetroNectin”, 20 µg/ml; Takara Bio), at a density of $1\text{-}2x10^5$ cells per well in complete RPMI plus IL-2 and 2-Mercaptoethanol as above. RV supernatants were thawed and added to the P14-containing wells at 100 µl per well. For non-transduced control, 100 µl of complete DMEM was added instead of RV supernatant. Spinfection was performed at 2000 xg for 60 minutes with no brake. Immediately following the spin, the plates were placed in a 37 °C incubator for 1-2 days. Transduction efficiency was confirmed by flow cytometry detection of mCherry or GFP fluorescent protein expression (15-20% positive for KLF3-OE and 40-50% for Ctl). Successfully transduced

cells were sorted as mCherry+ or GFP+ using Sony MA900 cell sorter, followed by adoptive transfer into chronic LCMV-infected or tumor-bearing mice as described.

Chronic LCMV infection model

All chronic LCMV infection experiments were performed following IACUC guidelines under the protocol #2019A00000055-R2. Age- and sex-matched Rag1-/- mice were anesthetized and infected with the LCMV clone 13 virus strain ($2x10^6$ PFU in 300 µl sterile RPMI per mouse) by retro-orbital intravenous injection. For KLF3-OE experiments, transduced P14 cells (Thy1.1+1.2- or Thy1.1+1.2+) were co-adoptively transferred into congenically distinct (Thy1.1-1.2+) recipient mice on day 2 post-infection, at a 1:1 ratio with $2.5x10^4$ cells of each type (KLF3-OE mCherry+ or Ctl-GFP+). Expansion of P14 cells was monitored by bleeding at effector (day 8-10) and chronic timepoints to confirm infection. Mice were humanely euthanized at the indicated experiment endpoints, followed by harvesting and processing of spleen, liver, and lungs previously described [22,32]. Single cell suspensions of each tissue were used for flow cytometry analysis or sorting as indicated.

For TGFβR1i+BMPa treatment experiments (**Fig. 7**), chronically infected mice were treated with either Mock (DMSO in sterile PBS) or RepSox ("TGFβR1i", 5 mg per kg in sterile PBS) and SB4 ("BMPa", 5 mg per kg in sterile PBS) via intraperitoneal injection every 2 days for a total of 4 doses as previously described [22]. For immune checkpoint blockade (ICB) treatment, mice received anti-PD-L1 (200 µg per mouse in sterile PBS; BioXCell) every 3 days for a total of 3 doses. Mice were randomized into treatment groups prior to onset, and blinding was not used during the administration of treatments. Mice were humanely euthanized 1-2 days after the final anti-PD-L1 dose, and tissues were harvested and processed as previously described [22].

***Ex vivo* GP33 peptide stimulation for P14 functional analysis**

To measure cytokine production of P14 cells from *in vitro*, chronic LCMV and tumor experiments, single-cell suspensions were stimulated with GP33 peptide (0.3 µg/ml) plus protein transport inhibitors (brefeldin A "GolgiPlug" and monensin "GolgiStop"; BD Biosciences) for 5 hours in a 37

°C incubator, followed by fixation and permeabilization for antibody staining of cytokines. To measure degranulation activity, anti-mouse CD107a-BV421 antibody (Clone 1D4B, Cat. 121617; BioLegend) was included with the stimulation cocktail.

Spectral flow cytometry and staining

All cell samples used for spectral flow cytometry were stained with antibody panels and run on Cytek Aurora 5L or 4L-UV cytometers, followed by analysis using FlowJo software (Version 10.8.1). Surface staining was performed for at least 15 minutes in FACS buffer (PBS plus 4% FBS; Gibco). Staining of dead cells was performed using Live/Dead Aqua (Ghost Dye Violet 510; Cytek BioSciences). The following anti-mouse surface antibodies were used throughout this study (all from BioLegend): CD8a-PerCP/Cy5.5 (Clone 53-6.7, Cat. 100733), CD8a-BV421 (Clone 53-6.7, Cat. 100737), CD8a-BV785 (Clone 53-6.7, Cat. 100749), CD107a-BV421 (Clone 1D4B, Cat. 121617), Ccr7-BV650 (Clone 4B12, Cat. 120137), Cx3cr1-BV711 (Clone SA011F11, Cat. 149031), Ly108-Pacific Blue (Clone 330-AJ, Cat. 134608), PD-1-APC/Cy7 (Clone 29F.1A12, Cat. 135223), PD-1-PE/Cy7 (Clone 29F.1A12, Cat. 135215), Thy1.1-BV605 (Clone OX-7, Cat. 202537), Thy1.1-FITC (Clone OX-7, Cat. 202503), Thy1.2-PerCP/Cy5.5 (Clone 53-2.1, Cat. 140321), Tim3-PE (Clone RMT3-23, Cat. 119703), and Tim3-PE/Cy7 (Clone RMT3-23, Cat. 119715). To confirm P14 cell antigen specificity, GP33 tetramer on APC (NIH Tetramer Core Facility) was included as a surface marker.

For intracellular staining (ICS), surface-stained cells were fixed in 4% paraformaldehyde solution (ThermoFisher) for at least 20 minutes or overnight, followed by permeabilization using the eBioscience™ Foxp3/ Transcription Factor Staining Buffer Set (Invitrogen). ICS was performed for at least 30 minutes in 1X permeabilization buffer at room temperature. The following anti-mouse intracellular antibodies were used throughout this study: Ki67-BUV737 (Clone SolA15, Cat. 367-5698-82; Invitrogen), Tcf1-BV421 (Clone S33-966, Cat. 566692; BD Biosciences). From BioLegend: DYKDDDDK Tag (FLAG)-PE (Clone L5, Cat. 637309), Granzyme B-Alexa Fluor 647 (Clone GB11, Cat. 515405), Granzyme B-Pacific Blue (Clone GB11, Cat.

515407), IFN-γ-APC (Clone XMG1.2, Cat. 505809), Perforin-PE (Clone S16009A, Cat. 154305), Puromycin-Alexa Fluor 647 (Clone 2A4, Cat. 381507), and TNF-α-BV650 (Clone MP6-XT22, Cat. 506333).

Cell sorting

All sorted cells throughout this study were isolated using a Sony MA900 Multi-Application Cell Sorter. The indicated populations were isolated by antibody staining or fluorescent protein expression and sorted into collection tubes prior to downstream analysis.

***In vitro* P14 tumor killing assay**

Tumor killing activity of *in vitro*-stimulated P14 cells was performed as previously described [22,32]. CT2A-GP33 glioma tumor cells (kindly received from Dr. Hiroshi Nakashima at Harvard University) were grown in complete RPMI medium and harvested from confluent flasks one day prior to co-culture with P14 cells. The CT2A cells were labeled with Cell Trace Violet ("CTV"; 1 uM, MilliporeSigma), then seeded into 96-well flat-bottom plates at a density of $6x10^4$ viable cells per 100 ul of complete RPMI. Plates were incubated overnight at 37 °C, 5% CO_2 to allow monolayer formation. The following day, *in vitro*-stimulated, transduced P14 cells (originally sorted one day after RV transduction as Ctl-GFP+ or KLF3-OE mCherry+) were collected on day 14 of chronic GP33 + TGFβ1 stimulation and seeded onto the CT2A wells ($6x10^4$ viable P14 cells per 100 ul of complete RPMI). The co-culture plates were incubated overnight for at least 18 hours at 37 °C and 5% CO_2. After overnight incubation, the wells were harvested and stained for spectral flow cytometry analysis. Tumor killing activity was determined by measuring the number of dead CTV+ CT2A tumor cells per 100 viable CD8+ cells by flow cytometry.

***In vivo* subcutaneous B16-F10 tumor model**

For *in vivo* subcutaneous tumor experiments in **Fig. 3**, GP33-expressing B16-F10 melanoma tumor cells (kindly received from Dr. Andreas Wieland at The Ohio State University) were first cultured in T75 tissue culture flasks and grown in complete DMEM medium (10% FBS, 1X penicillin/streptomycin). Male or female Thy1.2+ C57BL/6 mice at least 8 weeks old were injected

subcutaneously with $2.5x10^5$ viable B16-F10-GP33 tumor cells into the right or left flank. Once tumors became palpable (≥50-100 mm^3), congenically distinct P14 CD8+ T cells (Thy1.1+1.2- or Thy1.1+1.2+) were isolated and used for RV transduction as described above. One day following RV transduction, Ctl or KLF3-OE P14 cells were respectively sorted as GFP+ or mCherry+ and adoptively transferred into tumor-bearing recipient mice ($1.0x10^5$ P14 cells for single-transfer experiments, or a mixture of $9.0x10^4$ Ctl-GFP+ and $9.0x10^4$ KLF3-OE mCherry+ P14 cells for co-adoptive transfer experiments). Recipient groups were confirmed to have no significant difference in average tumor volume on the day prior to adoptive transfer. Tumor growth measurements were tracked daily via caliper, and mice were humanely euthanized once tumors reached early removal criteria size (1.6 cm length). At the indicated harvest timepoints, tumors or draining lymph nodes (tDLNs) were collected and processed as previously described [22,75], then used for phenotypic and functional analyses via spectral flow cytometry.

Ultra-low input RNA sequencing (ULI-RNAseq)

For RNA sequencing of Ctl or KLF3-OE CD8+ T cells, transduced P14 cells were first isolated from spleens of LCMV-infected mice using the Sony MA900 cell sorter. RNA was isolated from sorted cell pellets using the AllPrep DNA/RNA Micro Kit (Qiagen), from a range of ~$2.0-5.0x10^4$ cells per sample. The RNA samples were submitted for ultra-low input RNA sequencing using the GENEWIZ sequencing service (Azenta). Basic analysis was performed using our in-house pipeline [76]. Raw fastq was trimmed using TrimGalore and cutadapt to remove automatically detected adapters. The trimmed reads were aligned to mouse reference genome GRCm38 with hisat2 v2.1.0 [77]. Gene wise counts were generated with featureCounts from the subread package v1.5.1 [78] for genes annotated by ensembl Mus_musculus.GRCm38.102. We kept genes with at least 2000 counts across the samples. We batch corrected reads using ComBat_seq from sva.

Differential gene expression analysis

The batch corrected reads were used for differential gene expression analysis (DESeq2) and principal component analysis (PCA) using Partek Flow software (v12). Significant differentially

731 expressed genes (DEGs) were defined as those with fold change ≥ 1.5 (upregulated) or ≤ -1.5
732 (downregulated) and p<0.05 in KLF3-OE versus Ctl P14 cells. DEG lists were used for gene set
733 enrichment analysis against published TEX signatures [44] using UCSD and Broad Institute GSEA
734 software [79,80], and gene ontology (GO) and pathway enrichment analyses using Enrichr software
735 [81–83]. Representative heatmaps for progenitor and cytolytic TEX signature genes were generated
736 using Broad Institute Morpheus software [84].

737 **Whole genome bisulfite sequencing (WGBS)**

738 Whole genome bisulfite sequencing (WGBS) was performed on genomic DNA from sorted
739 transduced P14 cells, which was isolated using the AllPrep DNA/RNA Micro Kit (Qiagen). The
740 DNA samples were submitted for WGBS using Novogene sequencing service. We assessed raw
741 read QC with FastQC v0.11.8 before trimming and after trimming. Trimming was performed with
742 TrimGalore v0.4.5 and cutadapt v1.18 specifying RRBS and Illumina with a quality cutoff of 20.
743 Quality and adapter trimmed reads were aligned to bismark generated indexes for GRCh38 with
744 bismark v0.22.1 using bowtie2 v2.3.5.1 with options " --N 1 --L 15 -D 50 --score_min L,-0.6,-0.6 -
745 p 10 --X 600". Methylations were extracted using bismark_methylation_extractor. Reports were
746 generated with bismark2report. Alignment bam were sorted and indexed with samtools v1.9. Final
747 summary report was generated with bismark2summary for all samples.

748 **Differential DNA methylation analysis**

749 Differentially methylated regions (DMRs) were identified from mm10 WGBS data using DSS.
750 Bismark coverage files were converted to DSS input using chromosome, CpG coordinate,
751 methylated read count, and total CpG coverage, calculated as methylated plus unmethylated
752 reads. CpGs with coverage <5 reads were excluded, duplicate CpG entries were collapsed by
753 retaining the highest-coverage record, and analyses were restricted to CpGs shared across
754 samples within each comparison. Differential methylation testing was performed chromosome-
755 wise using DMLtest with smoothing enabled. Candidate DMRs were called using callDMR with a
756 CpG-level p < 0.01, minimum region length of 50 bp, and at least three CpGs per region. To

reduce artifacts from unequal sequencing depth, regions were retained only if mean CpG coverage differed by no more than threefold between groups. For final downstream analysis, significant DMRs were defined as regions with $p < 0.05$ and an absolute methylation difference of ≥ 30% (hypermethylated DMRs) or ≤ -30% (hypomethylated DMRs) in KLF3-OE *versus* Ctl P14 cells. DMRs were annotated to the single-nearest gene within 1.5 kb using the Stanford Genomic Regions Enrichment of Annotations Tool GREAT v4 [85]. DMR snapshots were generated using custom Python scripts from Bismark coverage files by averaging CpG methylation percentages across each group and plotting CpG-level methylation across selected regions.

Puromycin incorporation assay

To assess protein translation activity of P14 cells during *ex vivo* GP33 peptide stimulation, puromycin (10 ug/ml, MilliporeSigma) was added to the P14 cells during the 5-hour peptide stimulation at the last 20 minutes. After 20 minutes, the cells were surface stained and fixed as described above. During intracellular staining, a puromycin-targeting antibody on Alexa Fluor 647 (Clone 2A4, Cat. 381507; BioLegend) was included in the staining buffer to label incorporated puromycin for detection via spectral flow cytometry.

CRISPR-Cas9 nucleofection for KLF3 knockout

To perform CRISPR-Cas9 deletion of *Klf3*, we followed an established method for Cas9-ribonucleoprotein (RNP) nucleofection [29,86]. Naive P14 CD8+ T cells were isolated from spleens and activated with anti-CD3 and anti-CD28 as described above. 1-2 days following activation, P14 cells were collected for nucleofection at $2x10^6$ cells per reaction. CRISPR-RNP complexes were formed by combining Cas9 nuclease protein (Genscript) at a 1:3 picomolar ratio with published single-guide RNA (sgRNA) sequences for the *Klf3* gene [29] or non-targeting scrambled control sequence (Synthego), followed by incubation for 10 minutes to allow complex formation. Two different regions in the *Klf3* gene were targeted by pre-established sgRNAs: 1) 5'-CCUCACUCACGGGAUACAGG-3', 2) 5'-GGCAGCUUACCACCGAGACA-3' [29]. The RNP complexes were added to the P14 cells resuspended in P4 buffer (Lonza), followed immediately

by electroporation using a Lonza Nucleofector. Nucleofected cells were recovered for 2-3 days in complete RPMI medium containing recombinant human IL-2 (200 IU/ml), IL-15 (10 ng/ml), IL-7 (2.5 ng/ml; Peprotech) and 2-Mercaptoethanol (50 μM) in a 37 °C incubator. Following recovery, the nucleofected P14 cells were collected for either *in vitro* chronic GP33 stimulation as described above, or used for co-adoptive transfer into chronic LCMV-infected mice ($3.5x10^4$ Scr-Ctl plus $3.5x10^4$ KLF3-KO cells per mouse).

To confirm CRISPR editing efficiency, DNA was isolated from the recovered P14 cells following nucleofection using the AllPrep DNA/RNA Micro Kit (Qiagen). PCR amplification was performed using primers around the Cas9-sgRNA target sites: 1) FP: 5'-CATCTCTCCCATAGCTTTTTGG -3', RP: 5'-GTACTTCTTAATGGGCGGACTG-3' [29], 2) FP: 5'-CCGGGAGGCCTGGTTTTAAT-3', RP: 5'-CACTGTGAACAGATCGGCCT-3' (NCBI Primer-Blast). The PCR products were run on 2% agarose gel and extracted from the gel bands using the Zymoclean Gel DNA Recovery Kit (Zymo). Isolated DNA from the PCR products were submitted for Sanger sequencing by The Ohio State University Comprehensive Cancer Center (CCC) Genomics Shared Resource. Editing efficiency was determined using EditCo Interference of CRISPR Edits (ICE) analysis tool v3.0 (Synthego) [87].

Statistical analyses

All statistical analyses of flow cytometry, qRT-PCR and targeted DNA methylation data were performed using GraphPad Prism software (v10.6). Comparisons between two groups were performed using Mann-Whitney U test (for unpaired samples) or paired t-test (for paired samples). Comparisons between three or more groups with single variable were performed by ordinary one-way ANOVA with Tukey's multiple comparisons test, or two-way ANOVA for two variables with Tukey's multiple comparisons test. Data were plotted as mean ± SEM, with significant p-value * *<0.05*, ** *<0.01*, *** *<0.001*, **** *<0.0001*. For RNA sequencing, data was statistically analyzed using PCA and DESeq2 via Partek Flow software (v12), GSEA using USCD and Broad Institute

GSEA software [79,80], and pathway enrichment using Enrichr tool [81–83]. For WGBS, statistical differential methylation analysis was performed as described above.

Data availability

Raw sequencing data from RNA or WGBS will be made publicly available at NCBI Gene Expression Omnibus (GEO) by the time of publication.

REFERENCES

1. Chung, H. K., McDonald, B. & Kaech, S. M. The architectural design of CD8+ T cell responses in acute and chronic infection: Parallel structures with divergent fates. *J Exp Med* 218, e20201730 (2021).
2. Rausch, L. & Kallies, A. Molecular Mechanisms Governing CD8 T Cell Differentiation and Checkpoint Inhibitor Response in Cancer. *Annual Review of Immunology* 43, 515–543 (2025).
3. Tonnerre, P. *et al.* Differentiation of exhausted CD8+ T cells after termination of chronic antigen stimulation stops short of achieving functional T cell memory. *Nat Immunol* 22, 1030–1041 (2021).
4. Baessler, A. & Vignali, D. A. A. T Cell Exhaustion. *Annual Review of Immunology* 42, 179–206 (2024).
5. Lan, X., Zebley, C. C. & Youngblood, B. Cellular and molecular waypoints along the path of T cell exhaustion. *Science Immunology* 8, eadg3868 (2023).
6. Miller, B. C. *et al.* Subsets of exhausted CD8+ T cells differentially mediate tumor control and respond to checkpoint blockade. *Nat Immunol* 20, 326–336 (2019).
7. Im, S. J. *et al.* Defining CD8+ T cells that provide the proliferative burst after PD-1 therapy. *Nature* 537, 417–421 (2016).

8. McManus, D. T. *et al.* An early precursor CD8+ T cell that adapts to acute or chronic viral infection. *Nature* 640, 772–781 (2025).
9. Hudson, W. H. *et al.* Proliferating Transitory T Cells with an Effector-like Transcriptional Signature Emerge from PD-1+ Stem-like CD8+ T Cells during Chronic Infection. *Immunity* 51, 1043-1058.e4 (2019).
10. Beltra, J.-C. *et al.* Developmental Relationships of Four Exhausted CD8+ T Cell Subsets Reveals Underlying Transcriptional and Epigenetic Landscape Control Mechanisms. *Immunity* 52, 825-841.e8 (2020).
11. Yousif, A. & Ghoneim, H. E. T cell exhaustion—a memory locked behind scars. *Nat Immunol* 22, 938–940 (2021).
12. Saadey, A. A., Yousif, A. & Ghoneim, H. E. Chapter Seven - Epigenetic programming of the immune responses in cancer. in *Cancer Immunology and Immunotherapy* (eds Amiji, M. M. & Milane, L. S.) 197–235 (Academic Press, 2022). doi:10.1016/B978-0-12-823397-9.00007-7.
13. Belk, J. A., Daniel, B. & Satpathy, A. T. Epigenetic regulation of T cell exhaustion. *Nat Immunol* 23, 848–860 (2022).
14. Ghoneim, H. E. *et al.* De Novo Epigenetic Programs Inhibit PD-1 Blockade-Mediated T Cell Rejuvenation. *Cell* 170, 142-157.e19 (2017).
15. Sen, D. R. *et al.* The epigenetic landscape of T cell exhaustion. *Science* 354, 1165–1169 (2016).
16. Pauken, K. E. *et al.* Epigenetic stability of exhausted T cells limits durability of reinvigoration by PD-1 blockade. *Science* 354, 1160–1165 (2016).
17. Philip, M. *et al.* Chromatin states define tumour-specific T cell dysfunction and reprogramming. *Nature* 545, 452–456 (2017).

18. Abdel-Hakeem, M. S. *et al.* Epigenetic scarring of exhausted T cells hinders memory differentiation upon eliminating chronic antigenic stimulation. *Nat Immunol* 22, 1008–1019 (2021).
19. Yates, K. B. *et al.* Epigenetic scars of CD8+ T cell exhaustion persist after cure of chronic infection in humans. *Nat Immunol* 22, 1020–1029 (2021).
20. Wherry, E. J. & Kurachi, M. Molecular and cellular insights into T cell exhaustion. *Nat Rev Immunol* 15, 486–499 (2015).
21. Shakiba, M. *et al.* TCR signal strength defines distinct mechanisms of T cell dysfunction and cancer evasion. *J Exp Med* 219, e20201966 (2021).
22. Saadey, A. A. *et al.* Rebalancing TGFβ1/BMP signals in exhausted T cells unlocks responsiveness to immune checkpoint blockade therapy. *Nat Immunol* 24, 280–294 (2023).
23. Vu, T. T. *et al.* Impaired B Cell Development in the Absence of Krüppel-like Factor 3. *J Immunol* 187, 5032–5042 (2011).
24. Hart, G. T., Hogquist, K. A. & Jameson, S. C. Krüppel-like Factors in Lymphocyte Biology. *J Immunol* 188, 521–526 (2012).
25. Kumar, B. V. *et al.* Human Tissue-Resident Memory T Cells Are Defined by Core Transcriptional and Functional Signatures in Lymphoid and Mucosal Sites. *Cell Reports* 20, 2921–2934 (2017).
26. Chen, Y. *et al.* BATF regulates progenitor to cytolytic effector CD8+ T cell transition during chronic viral infection. *Nat Immunol* 22, 996–1007 (2021).
27. Zhu, Z. *et al.* FOXP1 and KLF2 reciprocally regulate checkpoints of stem-like to effector transition in CAR T cells. *Nat Immunol* 25, 117–128 (2024).
28. Fagerberg, E. *et al.* KLF2 maintains lineage fidelity and suppresses CD8 T cell exhaustion during acute LCMV infection. *Science* 387, eadn2337 (2025).
29. Shen, J. *et al.* Krüppel-like factors 2 and 3 regulate T cell exhaustion by directing T cell residency and migration. *Immunity* 59, 1287-1305.e7 (2026).

30. DePauw, T. A. *et al.* KLF2 overrides the resident memory CD8 T cell differentiation program, in opposition to KLF3. *Proceedings of the National Academy of Sciences* 123, e2533700123 (2026).
31. Jadhav, R. R. *et al.* Epigenetic signature of PD-1+ TCF1+ CD8 T cells that act as resource cells during chronic viral infection and respond to PD-1 blockade. *Proceedings of the National Academy of Sciences* 116, 14113–14118 (2019).
32. Yousif, A. *et al.* Faithful modeling of terminal CD8^{+}T cell dysfunction and epigenetic stabilization in vitro. *JCI Insight* 10, (2025).
33. Satpathy, A. T. *et al.* Massively parallel single-cell chromatin landscapes of human immune cell development and intratumoral T cell exhaustion. *Nat Biotechnol* 37, 925–936 (2019).
34. Zheng, L. *et al.* Pan-cancer single-cell landscape of tumor-infiltrating T cells. *Science* 374, abe6474 (2021).
35. Wang, Y. *et al.* Proteotoxic stress response drives T cell exhaustion and immune evasion. *Nature* 647, 1025–1035 (2025).
36. Wu, X. *et al.* PD-1+ CD8+ T cells are exhausted in tumours and functional in draining lymph nodes of colorectal cancer patients. *Br J Cancer* 111, 1391–1399 (2014).
37. Galletti, G. *et al.* Two subsets of stem-like CD8+ memory T cell progenitors with distinct fate commitments in humans. *Nat Immunol* 21, 1552–1562 (2020).
38. Loschinski, R. *et al.* IL-21 modulates memory and exhaustion phenotype of T-cells in a fatty acid oxidation-dependent manner. *Oncotarget* 9, 13125–13138 (2018).
39. Zander, R. *et al.* Tfh-cell-derived interleukin 21 sustains effector CD8+ T cell responses during chronic viral infection. *Immunity* 55, 475-493.e5 (2022).
40. Qi, H. *et al.* Foxo3 Promotes the Differentiation and Function of Follicular Helper T Cells. *Cell Reports* 31, (2020).
41. Ojanen, M. J. T. *et al.* FURIN regulates cytotoxic T-lymphocyte effector function and memory cell transition in mice. *European Journal of Immunology* 53, 2250246 (2023).

42. Hendriks, J., Xiao, Y. & Borst, J. CD27 Promotes Survival of Activated T Cells and Complements CD28 in Generation and Establishment of the Effector T Cell Pool. *J Exp Med* 198, 1369–1380 (2003).
43. Lee, S.-J. *et al.* 4-1BB and OX40 Dual Costimulation Synergistically Stimulate Primary Specific CD8 T Cells for Robust Effector Function. *J Immunol* 173, 3002–3012 (2004).
44. Hu, Y. *et al.* TGF-β regulates the stem-like state of PD-1+ TCF-1+ virus-specific CD8 T cells during chronic infection. *J Exp Med* 219, e20211574 (2022).
45. Xu, J. *et al.* BCOR and ZC3H12A suppress a core stemness program in exhausted CD8+ T cells. *J Exp Med* 222, e20241133 (2025).
46. Zhao, X. *et al.* The transcriptional cofactor Tle3 reciprocally controls effector and central memory CD8+ T cell fates. *Nat Immunol* 25, 294–306 (2024).
47. Shin, H. *et al.* A Role for the Transcriptional Repressor Blimp-1 in CD8+ T Cell Exhaustion during Chronic Viral Infection. *Immunity* 31, 309–320 (2009).
48. Skon, C. N. *et al.* Transcriptional downregulation of S1pr1 is required for the establishment of resident memory CD8+ T cells. *Nat Immunol* 14, 1285–1293 (2013).
49. Novák, J. *et al.* The sweet and the bitter sides of galectin-1 in immunity: its role in immune cell functions, apoptosis, and immunotherapies for cancer with a focus on T cells. *Semin Immunopathol* 47, 24 (2025).
50. Kouo, T. *et al.* Galectin-3 Shapes Antitumor Immune Responses by Suppressing CD8+ T Cells via LAG-3 and Inhibiting Expansion of Plasmacytoid Dendritic Cells. *Cancer Immunol Res* 3, 412–423 (2015).
51. Kasmani, M. Y. *et al.* Clonal lineage tracing reveals mechanisms skewing CD8+ T cell fate decisions in chronic infection. *J Exp Med* 220, e20220679 (2022).
52. Attwooll, C., Denchi, E. L. & Helin, K. The E2F family: specific functions and overlapping interests. *EMBO J* 23, 4709–4716 (2004).

53. Yang, Y. *et al.* ETS Transcription Factors in Immune Cells and Immune-Related Diseases. *International Journal of Molecular Sciences* 25, 10004 (2024).
54. Martinez, G. J. *et al.* The Transcription Factor NFAT Promotes Exhaustion of Activated CD8+ T Cells. *Immunity* 42, 265–278 (2015).
55. Dahabieh, M. S. *et al.* The prostacyclin receptor PTGIR is a NRF2-dependent regulator of CD8+ T cell exhaustion. *Nat Immunol* 26, 1139–1151 (2025).
56. Eaton, S. A. *et al.* A Network of Krüppel-like Factors (Klfs): Klf8 IS REPRESSED BY Klf3 AND ACTIVATED BY Klf1 IN VIVO*. *Journal of Biological Chemistry* 283, 26937–26947 (2008).
57. Yao, C. *et al.* BACH2 enforces the transcriptional and epigenetic programs of stem-like CD8+ T cells. *Nat Immunol* 22, 370–380 (2021).
58. Araki, K. *et al.* Translation is actively regulated during the differentiation of CD8+ effector T cells. *Nat Immunol* 18, 1046–1057 (2017).
59. Tan, T. C. J. *et al.* Suboptimal T-cell receptor signaling compromises protein translation, ribosome biogenesis, and proliferation of mouse CD8 T cells. *Proceedings of the National Academy of Sciences* 114, E6117–E6126 (2017).
60. Marchingo, J. M. & Cantrell, D. A. Protein synthesis, degradation, and energy metabolism in T cell immunity. *Cell Mol Immunol* 19, 303–315 (2022).
61. Riesenberg, B. P. *et al.* Stress-Mediated Attenuation of Translation Undermines T-cell Activity in Cancer. *Cancer Res* 82, 4386–4399 (2022).
62. Byl, W. V. D. *et al.* The CD8+ T cell tolerance checkpoint triggers a distinct differentiation state defined by protein translation defects. *Immunity* 57, 1324-1344.e8 (2024).
63. Aviner, R. The science of puromycin: From studies of ribosome function to applications in biotechnology. *Comput Struct Biotechnol J* 18, 1074–1083 (2020).

64. Wu, M., Wu, S., Chen, W. & Li, Y.-P. The roles and regulatory mechanisms of TGF-β and BMP signaling in bone and cartilage development, homeostasis and disease. *Cell Res* 34, 101–123 (2024).
65. Chu, T. *et al.* Precursors of exhausted T cells are pre-emptively formed in acute infection. *Nature* 640, 782–792 (2025).
66. Paley, M. A. *et al.* Progenitor and Terminal Subsets of CD8+ T Cells Cooperate to Contain Chronic Viral Infection. *Science* 338, 1220–1225 (2012).
67. Joshi, N. S. & Kaech, S. M. Effector CD8 T Cell Development: A Balancing Act between Memory Cell Potential and Terminal Differentiation. *J Immunol* 180, 1309–1315 (2008).
68. Morikawa, M. *et al.* BMP Sustains Embryonic Stem Cell Self-Renewal through Distinct Functions of Different Krüppel-like Factors. *Stem Cell Reports* 6, 64–73 (2016).
69. Bonilla-Claudio, M. *et al.* Bmp signaling regulates a dose-dependent transcriptional program to control facial skeletal development. *Development* 139, 709–719 (2012).
70. Zhu, X., Li, Q. & Zhu, X. Mechanisms of CAR T cell exhaustion and current counteraction strategies. *Front. Cell Dev. Biol.* 10, (2022).
71. Chow, A., Perica, K., Klebanoff, C. A. & Wolchok, J. D. Clinical implications of T cell exhaustion for cancer immunotherapy. *Nat Rev Clin Oncol* 19, 775–790 (2022).
72. Sakamoto, Y. *et al.* Long-read whole-genome methylation patterning using enzymatic base conversion and nanopore sequencing. *Nucleic Acids Res* 49, e81 (2021).
73. Napoleone, A. *et al.* Overcoming lentiviral delivery limitations in hard-to-transduce suspension cells for genome-wide CRISPR screening. *Molecular Therapy Advances* 34, (2026).
74. Kurachi, M. *et al.* Optimized retroviral transduction of mouse T cells for in vivo assessment of gene function. *Nat Protoc* 12, 1980–1998 (2017).
75. Buchwald, Z. S. *et al.* Tumor-draining lymph node is important for a robust abscopal effect stimulated by radiotherapy. *J Immunother Cancer* 8, (2020).

76. Gadepalli, V. S., Ozer, H. G., Yilmaz, A. S., Pietrzak, M. & Webb, A. BISR-RNAseq: an efficient and scalable RNAseq analysis workflow with interactive report generation. *BMC Bioinformatics* 20, 670 (2019).
77. Kim, D., Langmead, B. & Salzberg, S. L. HISAT: a fast spliced aligner with low memory requirements. *Nat Methods* 12, 357–360 (2015).
78. Liao, Y., Smyth, G. K. & Shi, W. featureCounts: an efficient general purpose program for assigning sequence reads to genomic features. *Bioinformatics* 30, 923–930 (2014).
79. Subramanian, A. *et al.* Gene set enrichment analysis: A knowledge-based approach for interpreting genome-wide expression profiles. *Proceedings of the National Academy of Sciences* 102, 15545–15550 (2005).
80. Mootha, V. K. *et al.* PGC-1α-responsive genes involved in oxidative phosphorylation are coordinately downregulated in human diabetes. *Nat Genet* 34, 267–273 (2003).
81. Chen, E. Y. *et al.* Enrichr: interactive and collaborative HTML5 gene list enrichment analysis tool. *BMC Bioinformatics* 14, 128 (2013).
82. Kuleshov, M. V. *et al.* Enrichr: a comprehensive gene set enrichment analysis web server 2016 update. *Nucleic Acids Res* 44, W90–W97 (2016).
83. Xie, Z. *et al.* Gene Set Knowledge Discovery with Enrichr. *Current Protocols* 1, e90 (2021).
84. Starruß, J., de Back, W., Brusch, L. & Deutsch, A. Morpheus: a user-friendly modeling environment for multiscale and multicellular systems biology. *Bioinformatics* 30, 1331–1332 (2014).
85. McLean, C. Y. *et al.* GREAT improves functional interpretation of cis-regulatory regions. *Nat Biotechnol* 28, 495–501 (2010).
86. Nüssing, S. *et al.* Efficient CRISPR/Cas9 Gene Editing in Uncultured Naive Mouse T Cells for In Vivo Studies. *J Immunol* 204, 2308–2315 (2020).
87. Conant, D. *et al.* Inference of CRISPR Edits from Sanger Trace Data. *The CRISPR Journal* 5, 123–130 (2022).

FIGURES:

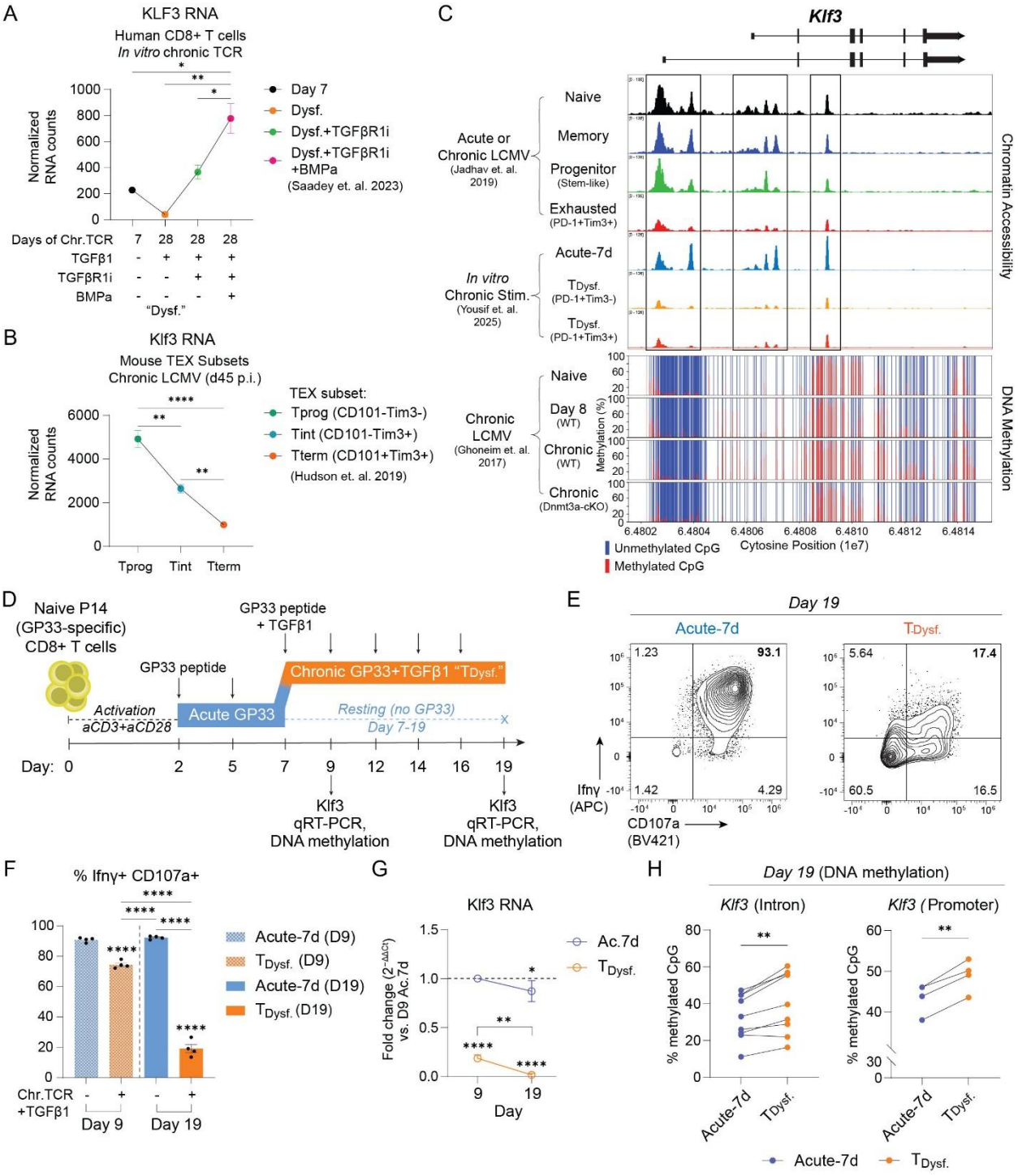

Fig. 1. KLF3 transcription factor is epigenetically silenced in terminally exhausted CD8+ T cells. (**A**) Normalized RNA counts for KLF3 within *in vitro*-stimulated human cord blood-derived CD8+ T cells on day 7 or day 28 of chronic TCR stimulation [22]. Chronically stimulated cells received TGFβ1 alone ("dysfunctional = Dysf.") or were treated with TGFβ receptor-1 inhibitor

(TGFβR1i) with or without BMP agonist (BMPa) to block terminal dysfunction. (**B**) RNA counts for KLF3 within mouse exhausted CD8+ T cell (TEX) subsets during chronic LCMV infection on day 45 p.i. [9] (Progenitor "Tprog": PD-1+ CD101- Tim3-, Intermediate "Tint": PD-1+ CD101-Tim3+, Terminally Exhausted "Tterm": PD-1+ CD101+Tim3+). (**C**) Integrative Genomics Viewer (IGV) snapshots showing accessible chromatin peaks at the *Klf3* locus in murine naive, memory, stem-like progenitor (PD-1+CXCR5+Tim3-) or exhausted (PD-1+CXCR5-Tim3+) CD8+ T cells [31], or *in vitro* acutely or chronically stimulated mouse P14 (GP33-specific) CD8+ T cells [32] ("Acute-7d": GP33 peptide stimulation for 7 days followed by rest until day 19, "$T_{Dysf.}$": chronic GP33 plus TGFβ1 for 19 days). Peaks were overlaid with DNA methylation profiles within the *Klf3* locus for naive, wild-type (WT) effector ("Day 8"), wild-type exhausted ("Chronic"), or Dnmt3a conditional knockout ("Chronic Dnmt3a-cKO") virus-specific CD8+ T cells from chronic LCMV infection [14]. (**D**) Schematic for *in vitro* chronic GP33 peptide stimulation of P14 CD8+ T cells [32], during which Klf3 RNA expression (by quantitative real-time PCR, "qRT-PCR") and DNA methylation were tracked throughout the stimulation period. (**E**) Representative FACS plots showing Ifnγ and CD107a expression levels on day 19, and (**F**) bar graph showing frequencies of Ifnγ+ CD107a+ Acute-7d or $T_{Dysf.}$ P14 cells on day 9 or 19 of *in vitro* chronic stimulation. (**G**) Fold change in average cycle threshold ($2^{-\Delta\Delta Ct}$) of Klf3 RNA in Acute-7d or $T_{Dysf.}$ P14 cells compared to day 9 Acute-7d levels. (**H**) Average frequency of methylated CpG sites within *Klf3* intron or promoter differentially methylated regions (DMRs) for Acute-7d or $T_{Dysf.}$ P14 cells on day 19 of chronic stimulation. Each connected line represents a single CpG site. Data for (**D-H**) represents 2-3 biologically independent experiments, with n=4 technical replicates for flow cytometry data or n=2 replicates for qRT-PCR and DNA methylation analyses. Data with error bars shown as mean ± SEM. Comparisons were determined by one-way ANOVA with Tukey's multiple comparisons test (**A, B**, **F, G**) or paired t-test (**H**). Significant p-values are shown relative to day 9 Acute-7d or as indicated. * *p <0.05*, ** *p <0.01*, **** *p<0.0001*.

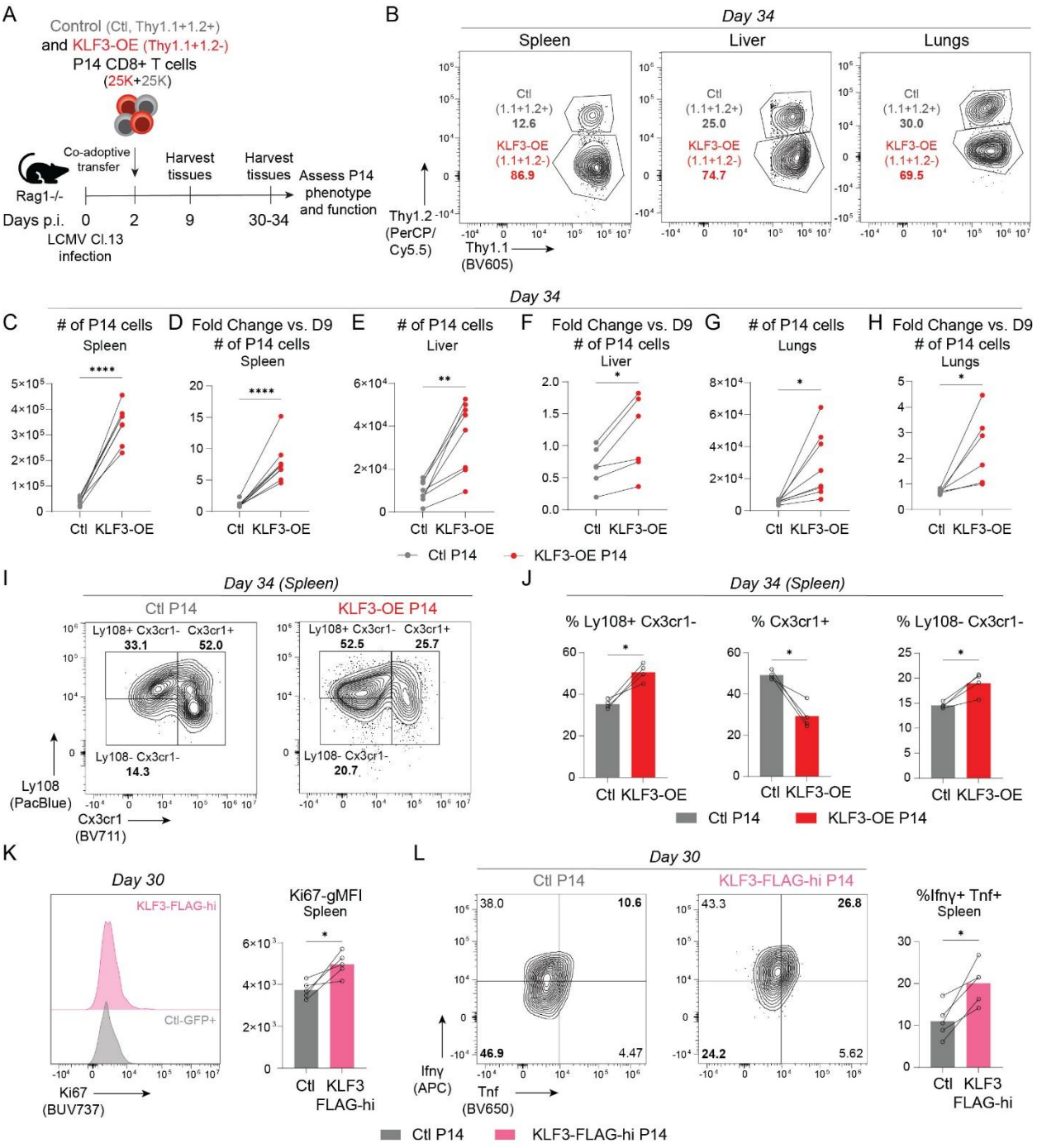

Fig. 2. Restoring KLF3 in virus-specific CD8+ T cells maintains progenitor-like state during chronic LCMV infection. (**A**) Schematic for co-adoptive transfer of congenically distinct, retrovirally transduced P14 CD8+ T cells into Rag1-deficient (Rag1-/-) mice that received LCMV clone 13 (chronic) infection. Control (Ctl) GFP+ (Thy1.1+1.2+) and KLF3-overexpressing (KLF3-OE) mCherry+ (Thy1.1+1.2-) P14 CD8+ T cells were combined 1:1 with $2.5x10^4$ of each cell type, then transferred intravenously into mice on day 2 p.i.. Spleens, livers, and lungs were analyzed on day 9 or day 30-34 p.i.. (**B**) Representative FACS plots showing frequencies of Ctl

(Thy1.1+1.2+) and KLF3-OE (Thy1.1+1.2-) P14 populations in spleens, livers, and lungs on day 34 p.i.. (**C**) Summary plot showing numbers and (**D**) fold change in number versus day 9 for Ctl or KLF3-OE P14 cells in spleens, (**E, F**) livers, and (**G, H**) lungs on day 34 p.i.. Paired values for the same samples are indicated by connecting lines. (**I**) Representative FACS plots showing Ly108 versus Cx3cr1 expression levels, and (**J**) bar graphs showing frequencies of Ly108 and Cx3cr1-expressing populations (Ly108+ Cx3cr1-, Cx3cr1+, and Ly108- Cx3cr1-) within Ctl or KLF3-OE P14 cells in spleens on day 34 p.i.. (**K**) Representative histograms and bar graph of Ki67 expression level (geometric mean fluorescence intensity, "gMFI") for KLF3-FLAG-hi and Ctl P14 cells on day 30 p.i.. (**L**) Representative FACS plots showing Ifnγ and Tnf cytokine expression levels, and bar graph showing frequencies of Ifnγ+ Tnf+ population within Ctl and KLF3-FLAG-hi P14 cells following 5-hr *ex vivo* GP33 peptide stimulation of splenocytes on day 30 p.i. Data represents 2-3 biologically independent experiments, with n=4-5 replicates per experiment. Data in (**C-H**) were pooled from 2 independent experiments. Comparisons were determined by paired t-test. Significant p-values are shown as indicated. * *p <0.05*, ** *p <0.01*, **** *p<0.0001*.

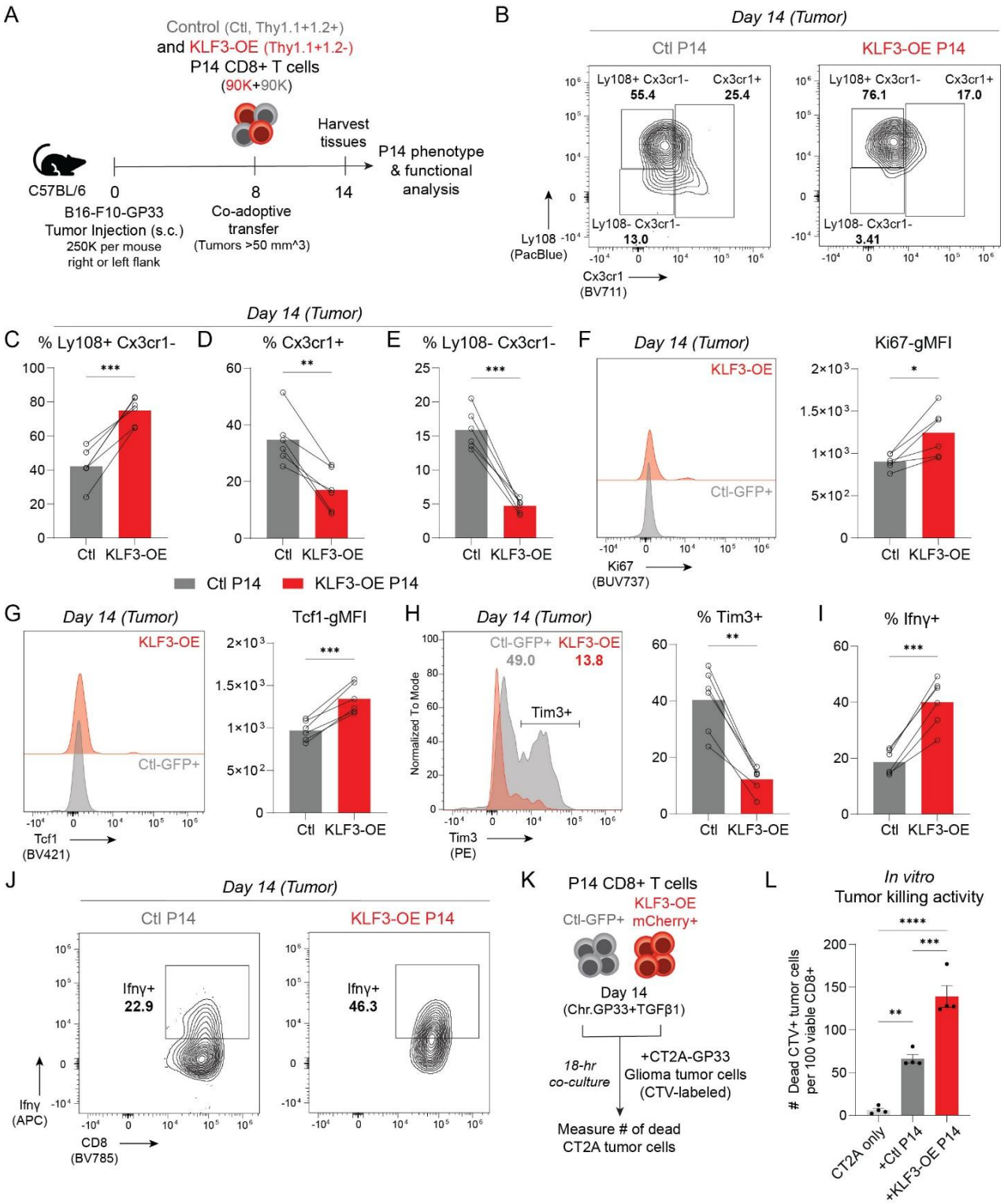

Fig. 3. KLF3-OE promotes stem-like programming and anti-tumor cytotoxicity of CD8+ T cells. (**A**) Schematic for co-adoptive transfer of congenically distinct Control GFP+ (Ctl, Thy1.1+1.2+) and KLF3-OE mCherry+ (Thy1.1+1.2-) P14 CD8+ T cells into C57BL/6 mice on day 8 after subcutaneous (s.c.) implantation with GP33-expressing B16-F10 melanoma cells into right or left flank, when tumor sizes were at least 50 mm^3. P14 cells were combined 1:1 with $9.0x10^4$

cells of each type, followed by intravenous injection into tumor-bearing mice. Tumors and inguinal draining lymph nodes (tDLN) were harvested on day 14 p.i.. (**B**) Representative FACS plots showing Ly108 versus Cx3cr1 expression levels, and (**C**) bar graphs showing frequencies of Ly108+ Cx3cr1-, (**D**) Cx3cr1+, or (**E**) Ly108- Cx3cr1- populations within Ctl or KLF3-OE P14 cells in tumors on day 14 p.i.. Paired values for the same samples are indicated by connecting lines. (**F**) Representative histograms and bar graphs showing expression levels (gMFI) of Ki67, or (**G**) Tcf1 in Ctl or KLF3-OE P14 cells in tumors on day 14. (**H**) Representative FACS plot and bar graph showing frequencies of Tim3+, or (**I, J**) Ifnγ+ populations within Ctl or KLF3-OE P14 cells in tumors on day 14. (**K**) Schematic for *in vitro* tumor killing assay of P14 cells [32], in which Ctl-GFP+ or KLF3-OE mCherry+ P14 cells were chronically stimulated with GP33 peptide and TGFβ1 for 14 days, followed by 18-hour co-culture with Cell Trace Violet (CTV)-labeled CT2A-GP33 glioma tumor cells. (**L**) Bar graph showing the number of dead CTV+ tumor cells following 18-hour co-culture with Ctl or KLF3-OE P14 cells, shown as ratio of dead tumor cells per 100 viable CD8+ T cells. Data represents 2-3 biologically independent experiments, with n=4=6 replicates per experiment. Data with error bars shown as mean ± SEM. Comparisons were determined by paired t-test (**C-I**) or one-way ANOVA with Tukey's multiple comparisons test (**L**). Significant p-values are shown as indicated. * *p <0.05*, ** *p <0.01*, *** *p<0.001*, **** *p<0.0001*.

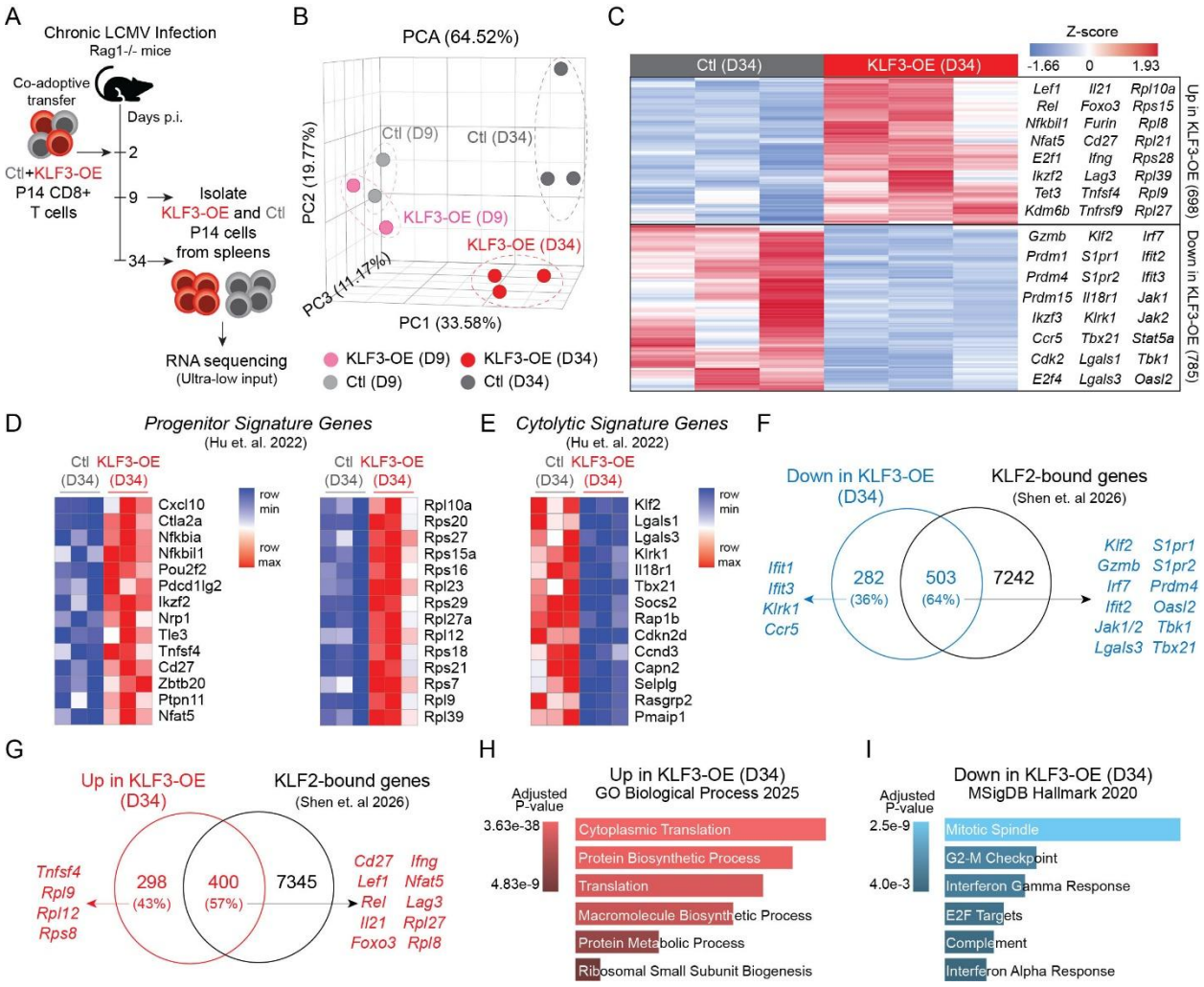

Fig. 4. Restoring KLF3 supports progenitor-associated transcriptional circuits in chronically stimulated CD8+ T cells. (**A**) Schematic for ultra-low input RNA sequencing of co-adoptively transferred KLF3-OE or Control (Ctl) P14 CD8+ T cells, which were isolated from spleens of chronic LCMV-infected Rag1-/- mice on day 9 or 34 p.i.. (**B**) Principal component analysis (PCA) plot comparing global transcriptional profiles between KLF3-OE or Ctl P14 cells on day 9 or day 34 p.i.. (**C**) Heatmap showing differentially expressed genes (DEGs) that were upregulated (fold change ≥ 1.5, p-value <0.05) or downregulated (fold change ≤ -1.5, p-value <0.05) in KLF3-OE P14 cells compared to Ctl cells on day 34 p.i., with example genes listed. DEGs were plotted based on relative Z-score of normalized RNA counts. (**D**) Heatmap showing example genes from progenitor, or (**E**) cytolytic TEX transcriptional signatures within P14 cells during chronic LCMV infection [44] and associated normalized RNA counts for Ctl or KLF3-OE P14 cells on day 34 p.i.. Red color indicates higher expression level and blue indicates lower expression. (**F**) Venn diagram showing overlap of downregulated or (**G**) upregulated DEGs in KLF3-OE P14 cells with genes that were bound by KLF2 in TEX cells during chronic LCMV infection [29], with example genes listed. (**H**) Summary plot for Gene Ontology (GO) biological processes that were enriched in upregulated DEGs, or (**I**) MSigDB Hallmark pathways that were enriched in downregulated DEGs in KLF3-OE cells on day 34 p.i.. Pathways are plotted in order

of p-value significance, and bar lengths pertain to number of genes in each pathway. RNA sequencing was performed on n=2-3 biologically independent samples per group, from 2 independent experiments. Statistical analysis was performed by PCA and DESeq2 using Partek Flow software. Heatmaps were generated using Partek Flow (**C**) or Broad Institute Morpheus (**D, E**) software [84]. Enrichment plots in (**H, I**) were generated using Enrichr software [81–83].

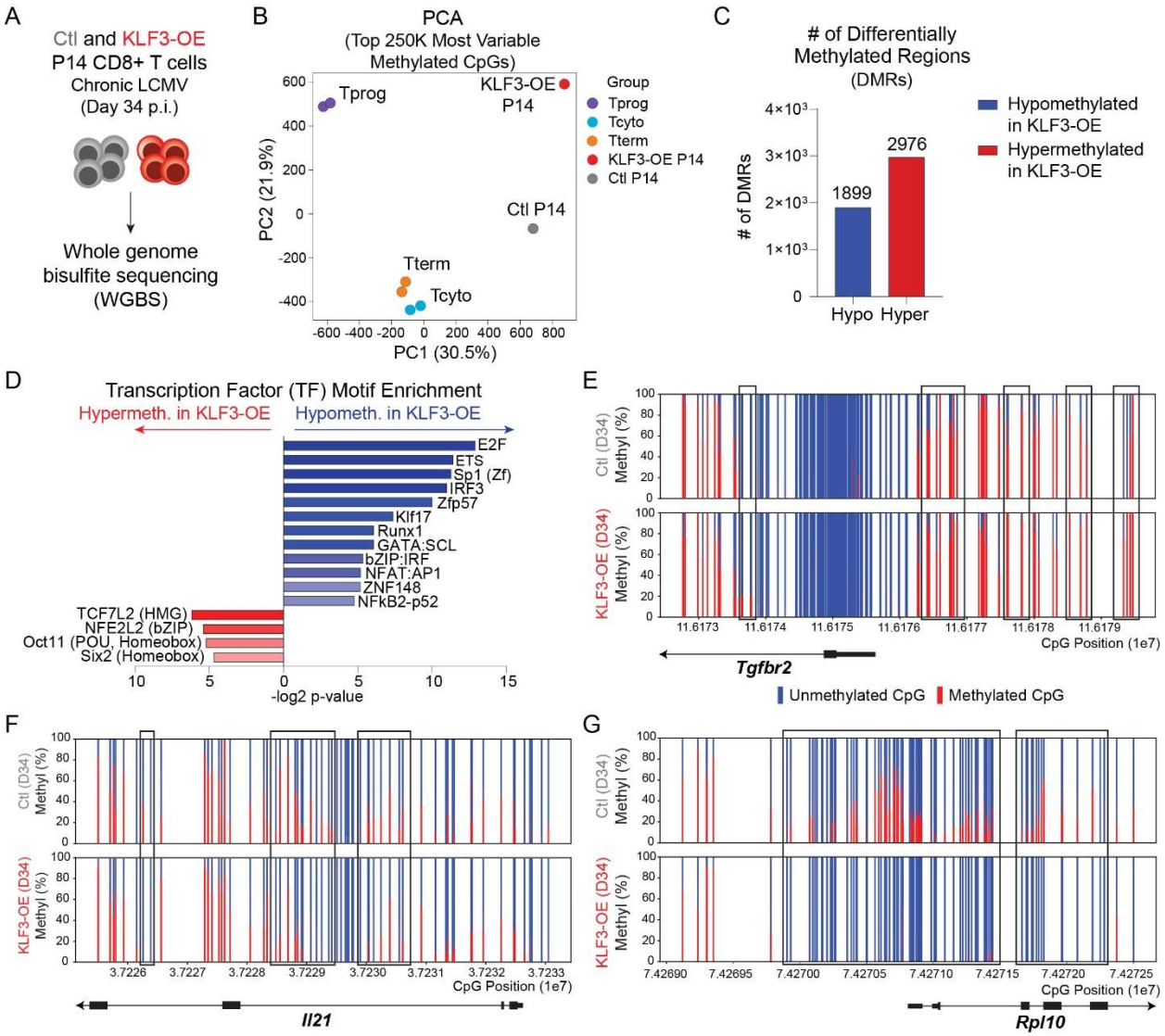

Fig. 5. KLF3-OE remodels exhaustion-associated DNA methylation programs in CD8+ T cells during chronic infection. (**A**) Schematic for whole genome bisulfite sequencing (WGBS) of Control (Ctl) or KLF3-OE P14 CD8+ T cells isolated from spleens of chronically infected Rag1-/- mice on day 34 p.i.. (**B**) Principal component analysis (PCA) plot comparing DNA methylation profiles of KLF3-OE and Ctl P14 cells to endogenous TEX subsets isolated from chronic LCMV-infected C57BL/6 mice (Tprog: PD-1+ Ly108+ Cx3cr1-, Tcyto: PD-1+ Cx3cr1+, Tterm: PD-1+ Ly108- Cx3cr1-). PCA was performed on the top 250,000 most variable methylated CpG sites among the samples. (**C**) Bar graph showing the number of differentially methylated regions (DMRs) with significantly lower (hypomethylated) or higher (hypermethylated) methylation in KLF3-OE P14 cells compared to Ctl cells. (**D**) Summary plot showing enriched transcription factor (TF) motifs within hypomethylated (blue) or hypermethylated (red) DMRs in KLF3-OE P14 cells, plotted based on -log2 p-value. Longer bars are more significant. (**E**) Snapshots showing frequency of DNA methylation in CpGs across *Tgfbr2*, (**F**) *Il21*, or (**G**) *Rpl10* gene loci for Ctl and KLF3-OE P14 cells. Each line represents a single CpG site, with red indicating higher methylation

frequency and blue indicating reduced methylation. WGBS was performed on n=1 sample per condition, with each sample originally pooled from 2 biologically independent LCMV infection experiments. Significant DMRs were defined as regions with $p<0.05$ and fold change in methylation ≥ 30% (hypermethylated) or ≤ -30% (hypomethylated) in KLF3-OE versus Ctl P14 cells.

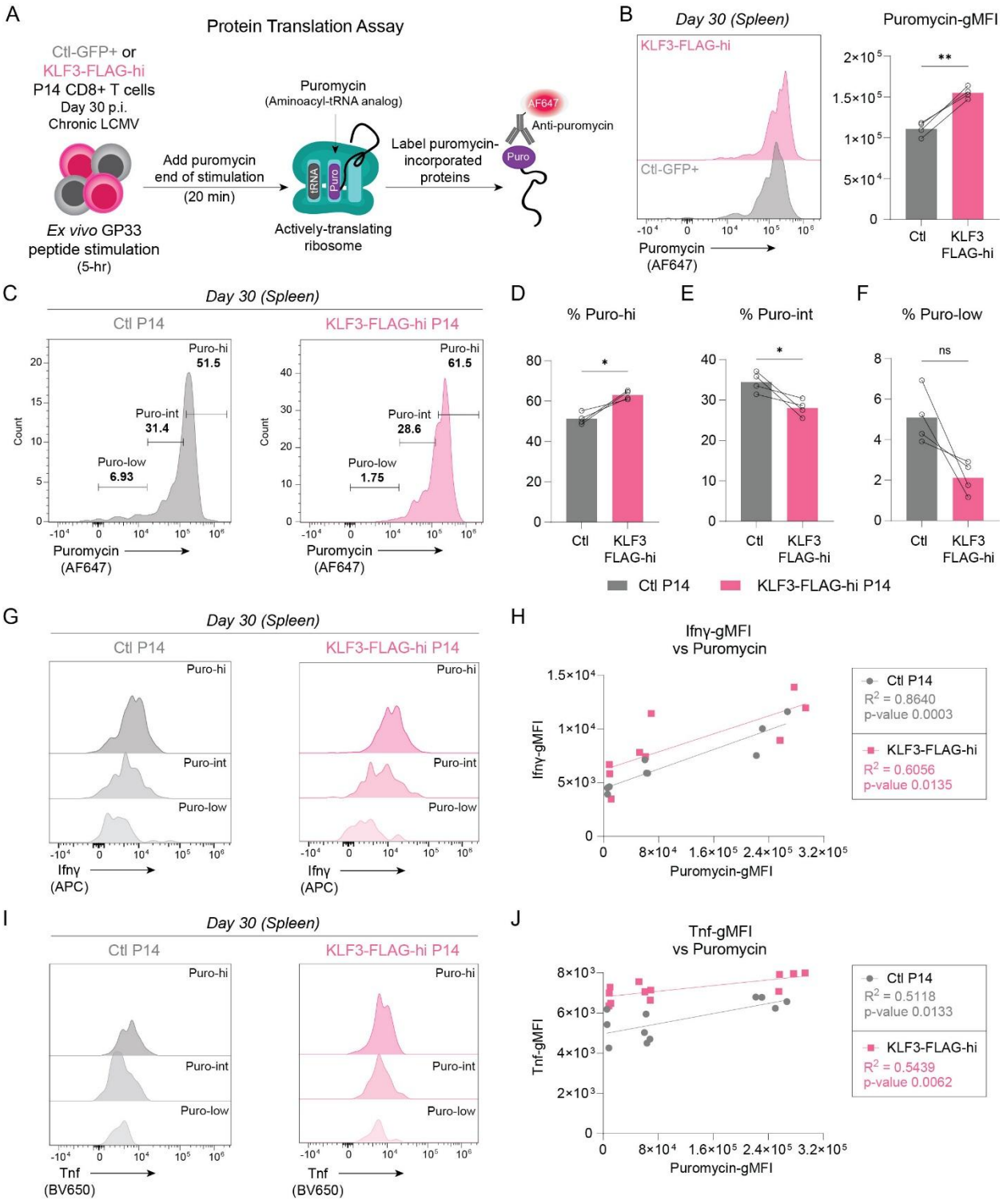

Fig. 6. KLF3 promotes protein translation activity in chronically stimulated CD8+ T cells. (**A**) Schematic for protein translation assay by puromycin incorporation. Splenocytes from chronic LCMV-infected Rag1-/- mice on day 30 p.i. were stimulated *ex vivo* with GP33 peptide for 5 hours, and puromycin was added to the cells 20 minutes prior to end of stimulation to incorporate into

actively-translating ribosomes. Puromycin-incorporated proteins were then labeled by puromycin-targeting antibody. (**B**) Representative histograms and bar graph showing puromycin staining (gMFI) within Control (Ctl-GFP+) or KLF3-FLAG-hi P14 cells on day 30 p.i.. Paired values from the same samples are shown by connecting lines. (**C**) Representative histograms showing frequencies of high, intermediate, and low puromycin-incorporating populations, and (**D**) bar graph showing frequencies of Puro-hi, (**E**) Puro-int, or (**F**) Puro-low populations within Ctl or KLF3-FLAG-hi P14 cells on day 30 p.i.. (**G**) Representative histograms showing Ifnγ or (**I**) Tnf expression levels, and (**H**) summary plot of Ifnγ or (**J**) Tnf versus puromycin levels (gMFI) for the Puro-hi, -int, and -low subsets within Ctl and KLF3-FLAG-hi P14 cells on day 30, with R^2 correlation and p-values listed. Data represents 2-3 biologically independent experiments, with n=4 replicates per experiment. Comparisons were determined by paired t-test (**B**, **D-F**) or simple linear regression goodness-of-fit test (**H**, **J**). Significant p-values are shown as indicated. * *p <0.05*, ** *p <0.01*, ns = not significant.

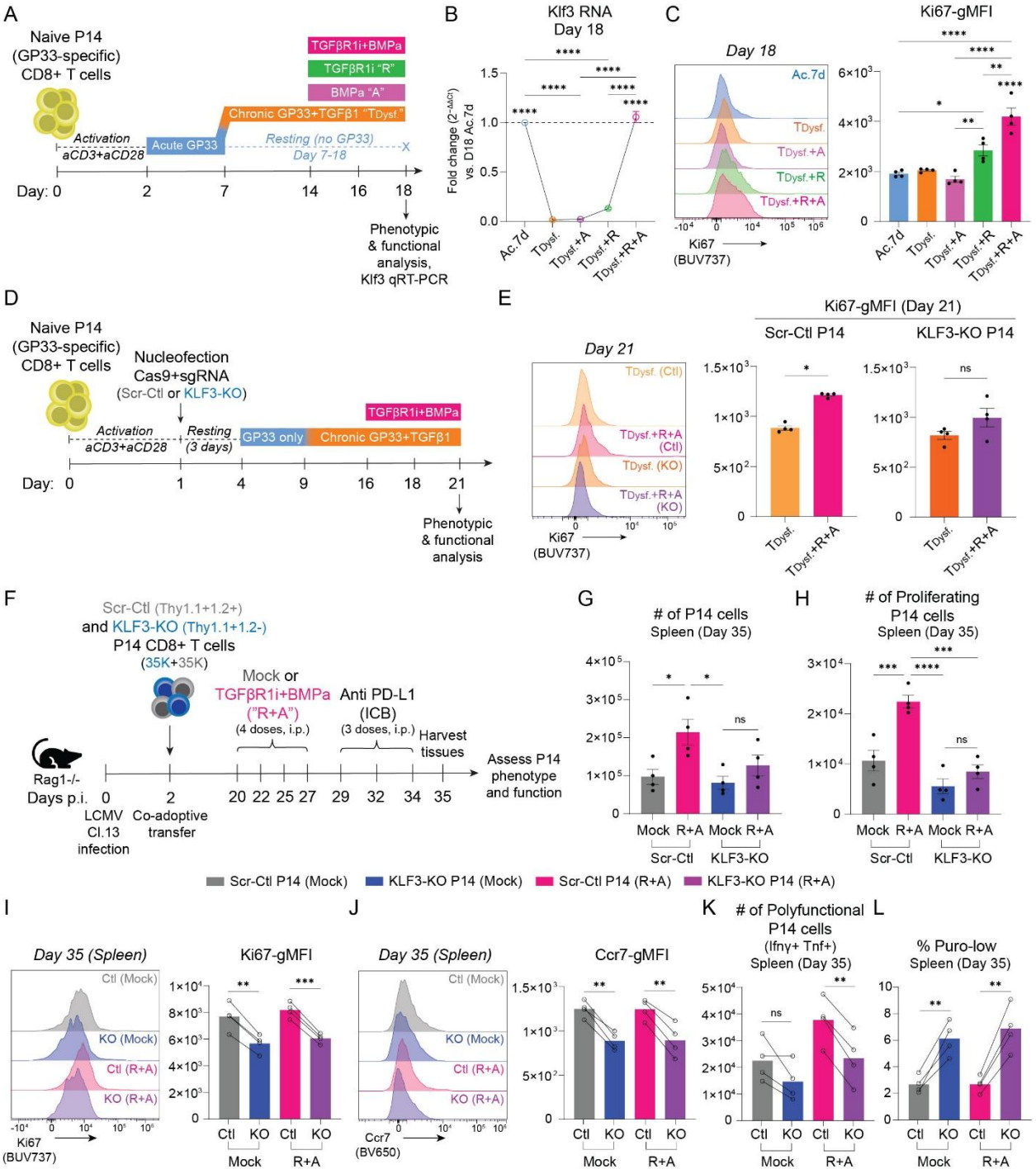

Fig. 7. BMP activation recovers KLF3-driven proliferative response of CD8+ T cells during ICB therapy. (**A**) Schematic for *in vitro* chronic stimulation of P14 CD8+ T cells [32] , during which $T_{Dysf.}$ (chronic GP33 + TGFβ1) cells were treated with BMP agonist (BMPa, "A"), TGFβ receptor 1-inhibitor (TGFβR1i, "R"), or combination ("R+A") from day 14 to 18 of chronic GP33 plus TGFβ1 stimulation. (**B**) Fold change in average cycle threshold ($2^{-\Delta\Delta Ct}$) of Klf3 RNA in Acute-7d, $T_{Dysf.}$, and treated $T_{Dysf.}$ P14 cells relative to Acute-7d levels on day 18. (**C**) Representative histograms and bar graph of Ki67 expression (gMFI) within Acute-7d or $T_{Dysf.}$ P14 cells on day 18. (**D**)

Schematic for *in vitro* chronic stimulation of P14 cells following nucleofection with Cas9+single-guide RNA (sgRNA) complexes, using either scrambled control (Scr-Ctl) or KLF3-targeting (KLF3-KO) guides [29]. P14 cells were treated with R+A combination from day 16 to day 21 of chronic GP33 plus TGFβ1 stimulation. (**E**) Representative histograms and bar graphs showing Ki67 expression (gMFI) in Scr-Ctl or KLF3-KO P14 cells on day 21 of *in vitro* stimulation. (**F**) Schematic for co-adoptive transfer of congenically distinct Scr-Ctl (Thy1.1+1.2+) or KLF3-KO (Thy1.1+1.2-) P14 CD8+ T cells ($3.5x10^4$ cells of each type) into Rag1-/- mice on day 2 post-chronic LCMV infection. Mice were treated intraperitoneally (i.p.) with either Mock or combined TGFβR1+BMPa (R+A) from day 20-27 p.i., followed by anti-PD-L1 (ICB) therapy given i.p. from day 29-34 p.i.. (**G**) Summary bar graphs showing total numbers of Scr-Ctl or KLF3-KO P14 cells, or (**H**) numbers of proliferating (Ki67+) P14 cells within spleens of Mock or R+A-treated mice on day 35 p.i. following ICB therapy. (**I**) Representative histograms and bar graphs showing Ki67, or (**J**) Ccr7 expression levels (gMFI) within Scr-Ctl or KLF3-KO P14 cells of Mock or R+A-treated mice on day 35 p.i. after ICB therapy. Paired values from the same samples are shown by connecting lines. (**K**) Bar graph showing numbers of polyfunctional (Ifnγ+ Tnf+), or (**L**) frequencies of low puromycin-incorporating (Puro-low) Scr-Ctl or KLF3-KO P14 cells from Mock or R+A-treated mice following *ex vivo* GP33 peptide stimulation of splenocytes on day 35 p.i.. Data represents 2-3 biologically independent experiments, with n=4 replicates per experiment. Data with error bars shown as mean ± SEM. Comparisons were determined by one-way ANOVA with Tukey's multiple comparisons test (**B, C, G, H**), Mann-Whitney U test (**E**), or paired t-test (**I-L**). Significant p-values are shown relative to $T_{Dysf.}$ (**B, C**) or as indicated. * *p <0.05*, ** *p <0.01*, *** *p<0.001*, **** *p<0.0001*, ns = not significant.

Supplementary Files

This is a list of supplementary files associated with this preprint. Click to download.

- SaadeyNatImmunolExtendedDataFigures.docx